

THESIS FOR THE DEGREE OF DOCTOR OF PHILOSOPHY
IN
THERMO AND FLUID DYNAMICS

**A Numerical Study of
Reacting Flows Using Finite
Rate Chemistry**

MOHAMMAD IRANNEZHAD

Division of Fluid Dynamics

Department of Applied Mechanics

CHALMERS UNIVERSITY OF TECHNOLOGY

Göteborg, Sweden, 2012

A Numerical Study of Reacting Flows Using Finite Rate Chemistry

MOHAMMAD IRANNEZHAD

ISBN 948-91-7385-776-5

© MOHAMMAD IRANNEZHAD, 2012

Doktorsavhandling vid Chalmers tekniska högskola

Ny serie nr 3457

ISSN 0346-718X

Division of Fluid Dynamics
Department of Applied Mechanics
Chalmers University of Technology
SE-412 96 Göteborg, Sweden

Phone: +46-(0)31-7721000

Fax: +46-(0)31-7723872

Printed at Chalmers Reproservice
Göteborg, Sweden, 2012

A Numerical Study of Reacting Flows Using Finite Rate Chemistry

MOHAMMAD IRANNEZHAD

Division of Fluid Dynamics
Department of Applied Mechanics
Chalmers University of Technology

Abstract

Fossil fuels will remain the main source of energy for mankind in the foreseeable future. Heat released in combustion of fossil fuels is always accompanied by emission of undesired pollutants. Environmental concerns have led to stringent emission rules for combustion industry specially for reducing the amount of NO_x production. Lean premixed combustion has increasingly gained interest in recent years as an approach toward reduced NO_x emissions by reducing the operating temperature. However, lean blow off limit and the tendency of the dynamic flame to become unstable present technical challenges. The low swirl burner concept is a rather new and promising design to stabilize lean premixed flames close to their flammability limit. Large Eddy Simulation together with a finite rate chemistry combustion model have been used here for numerical studies of a laboratory low swirl stabilized flame. The importance of the inlet boundary condition is investigated and an optimized approach is suggested. The flame stabilization mechanism is discussed and it is shown that the choice of the inlet boundary condition can significantly affect this mechanism.

Air transport is becoming more common and aviation contribution to anthropogenic CO_2 production will soon become prominent. Turbo-machinery efficiency in modern aircraft engines is close to perfection and innovative core designs are needed for significant efficiency improvements. Unsteady phenomena in the working cycle of a conceptual Pulse Detonation Engine is studied here using URANS and a finite rate chemistry combustion model. The limitations imposed by the unsteady flow at compressor side are compared for two alternative engine configurations.

Keywords: Combustion, Emissions, Lean premixed, Lean blow off, Dynamic flame, Low Swirl Burner, Large Eddy Simulation, Finite rate chemistry, Combustion modeling, Inlet boundary condition, Flame stabilization, Unsteady phenomena, Working cycle, URANS, Pulse Detonation Engine, Engine configuration

List of Publications

This thesis is based on the work contained in the following papers:

- I M. Irannezhad and L.-E. Eriksson, 2008, Flow-Flame Interactions in a Lean Premixed Low Swirl Burner, *The 7th International ERCOFTAC Symposium on Engineering Turbulence Modeling and Measurements-ETMM7*, June 4-6, Limassol, Cyprus
- II M. Irannezhad and L.-E. Eriksson, 2009, Large Eddy Simulation of a Lean Premixed Low Swirl Burner, *The 6th International Symposium on Turbulence and Shear Flow Phenomena-TSFP6*, June 22-24, Seoul, South Korea
- III M. Irannezhad, T. Grönstedt and L.-E. Eriksson, 2011, Limitations of Tube Filling in a Pulsed Detonation Engine, *The 20th ISABE Conference*, September 12-16, Göteborg, Sweden
- IV M. Irannezhad and L.-E. Eriksson, 2011, Large Eddy Simulation of Premixed Flames with Multi-step Global Reaction Mechanisms, *The 13th European Turbulence Conference-ETC13*, September 12-15, Warsaw, Poland
- V M. Irannezhad and L.-E. Eriksson, Importance of Boundary Conditions in LES of a Low Swirl Burner, 2012, *To be submitted for publication*

Division of work between authors

The respondent is the first author of all the papers on which this thesis is based. All the work is done by the respondent and all the papers are written by him and reviewed by co-authors. The theoretical work and code development presented in the papers were carried out in discussions with the supervisor, Professor Lars-Erik Eriksson. The ideas in paper III were discussed with professor Tomas Grönstedt.

Other relevant publications

- VI F. Giuliani, A. Lang, M. Irannezhad and T. Grönstedt, 2009, Effects of a Controlled Phase-Shift on the Outlet Conditions of a Set of Pulse Detonators, *The 19th ISABE Conference*, September 7-11, Montreal, Canada
- VII F. Giuliani, A. Lang, M. Irannezhad and A. Lundbladh, 2010, Pulse Detonation as an Option for Future Innovative Gas Turbine Combustion Technologies: a Concept Assessment, *The 27TH INTERNATIONAL CONGRESS OF THE AERONAUTICAL SCIENCES-ICAS2010*, September 19-24, Nice, France

Acknowledgments

The work on Low Swirl Burner was done within CeCoST (Center for Combustion Science and Technology) activities. Financial support from CeCoST and Swedish Energy Agency (STEM) is gratefully acknowledged.

Financial support for the work on PDE by the European Commission as part of the Integrated Project NEWAC (New Aero Engine Core Concepts, AIP-CT-2006-030876) is also highly acknowledged.

This work was carried out at the Department of Applied Mechanics, Division of Fluid Dynamics, at Chalmers University of Technology. The computations in this thesis have been done primarily on Chalmers Center for Computational Science and Engineering (C3SE).

This thesis could not have been written without inspiration, guidance and support from many people. First and foremost, my deep and sincere gratitude to my supervisor, Professor Lars-Erik Eriksson, for his support and constant source of motivation. His enlightening discussions and brilliant advice have made this work possible. I am specially grateful to Professor Tomas Grönstedt for inspiring discussions on PDE. Associate professor Gunnar Johansson is highly acknowledged for helping me understand fluid dynamics.

I would like to take this opportunity to thank the experimental campaign at Lund University, PhD student Per Petersson in particular, for providing the validation data used in this work. Special thanks to all colleagues and staff at the Division of Fluid Dynamics for the friendly environment they had made, making it possible to enjoy every moment of my studies.

My warmest and deepest sense of gratitude goes to my beloved Oldoos, my family and all friends for their unconditional support and understanding.

Nomenclature

Latin symbols

A	pre-exponential factor in Arrhenius expression
c	speed of sound
C	coefficient in combustion model
$C_{\varepsilon 1}$	constant in k-epsilon turbulence model
$C_{\varepsilon 2}$	constant in k-epsilon turbulence model
C_{μ}	constant in k-epsilon turbulence model
C_p	specific heat at constant pressure
C_s	constant in Smagorinsky subgrid model
C_v	specific heat at constant volume
D	diffusion coefficient
D_t	turbulent diffusion coefficient
e	internal energy
e_0	total internal energy
E_a	activation energy in Arrhenius expression
f	frequency
\mathcal{F}_j	Cartesian components of flux vector
h	enthalpy
h_0	total enthalpy
H_f	heat of formation
\mathcal{H}	source vector
J	species mass diffusion flux
k	turbulent kinetic energy
k_{sgs}	subgrid scale turbulent kinetic energy
Ka	Karlovitz number
Ka_{δ}	Karlovitz number based on inner layer thickness
l_t	turbulent length scale
$l_{t,max}$	turbulent length scale upper limit
ℓ	turbulent length scale
ℓ_F	flame thickness
M	Mach number, preconditioning matrix
M_{eff}	effective Mach number
p	pressure

P_k	turbulent production term
Pr	laminar Prandtl number
Pr_t	turbulent Prandtl number
q	heat release, heat diffusion flux
Q	state vector in conservative form
R	gas constant
Re	Reynolds number
RR	reaction rate
S_F	free stream velocity
S_{ij}	strain rate tensor
S_L	laminar flame speed
S_T	turbulent flame speed
s	stoichiometric ratio by weight
S	chemical source term
Sc	laminar Schmidt number
Sc_t	turbulent Schmidt number
t	time
t_η	Kolmogorov time scale
T	temperature, period
T_0	inner layer temperature
T_L	threshold temperature
t_F	flame time scale
u	velocity
u_t	turbulent velocity scale
U'	turbulent intensity
\vec{V}	diffusion velocity
\dot{w}	reaction rate
\bar{W}	mean reaction rate
x	Cartesian coordinate
X	mole fraction
Y	mass fraction
$Y_0^{Fu.}$	initial fuel mass fraction
$Y_L^{Fu.}$	threshold fuel mass fraction

Greek symbols

α	preconditioning under-relaxation factor, heat diffusivity
Δf	filter width
δ	inner layer thickness scaled by flame thickness
δ_{ij}	Kronecker delta
ε	dissipation of turbulent kinetic energy
η	Kolmogorov length scale
γ	specific heat ratio
λ	heat conductivity

μ	laminar dynamic viscosity
μ_t	turbulent eddy viscosity
ν	kinematic viscosity ($\nu = \mu/\rho$)
ν_{sgs}	subgrid scale kinematic viscosity
ϕ	equivalence ratio
ρ	density
σ_ε	constant in k-epsilon turbulence model
σ_k	constant in k-epsilon turbulence model
τ_c	chemistry time scale
τ_d	detonation/blowdown time
τ_f	fill time
τ_{ij}	viscous stress tensor
τ_p	purge time
τ_s	spark time
τ_t	turbulence time scale
v'	turbulent velocity scale
v_η	Kolmogorov velocity scale
ℓ_δ	inner layer thickness

Subscripts

sgs subgrid scale

Superscripts

(m) species m
 $-$ ensemble averaged quantity
 $'$ fluctuating quantity
 \sim Favre-filtered ensemble averaged quantity
 sgs subgrid scale

Abbreviations

CFD Computational Fluid Dynamics
CFL Courant-Friedrich-Lewy
DNS Direct Numerical Simulation
HPC High Pressure Compressor
HPT High Pressure Turbine
LES Large Eddy Simulation
LSB Low Swirl Burner
MPI Message Passing Interface
PDC Pulse Detonation Combustor
PDE Pulse Detonation Engine
PDF Probability Density Function
PDT Pulse Detonation Tube
ppm particle per million
ppmv particle per million by volume

RANS Reynolds Averaged Navier-Stokes
URANS Unsteady Reynolds Averaged Navier-Stokes
ZND Zeldovich-vonNeumann-Döring

Chemical Compounds

CH_4 methane
 CO carbon monoxide
 CO_2 carbon dioxide
 H_2 hydrogen
 H_2O water
 N_2 nitrogen
 NO_x nitrogen oxides
 O_2 oxygen

Contents

Abstract	iii
List of Publications	v
Acknowledgments	vii
1 Introduction	1
1.1 Motivation	1
1.2 Background	2
1.3 Low Swirl Burner	4
1.4 Modern Aircraft Engines	6
1.5 Thesis Objectives	7
2 Combustion	9
2.1 Combustion Modes	9
2.2 Detonation	12
2.2.1 ZND Structure of the Detonation Wave	13
2.3 Deflagration	15
2.3.1 Premixed Flame Structure	15
2.3.2 Laminar Flame Speed	16
2.4 Turbulent Combustion	17
2.5 Turbulent Flame Speed	18
2.6 Reduced Chemistry	19
2.7 Flame Stabilization	21
2.8 Turbulent Combustion Regimes	22
3 Methodology	25
3.1 Multi-Species Reacting Systems	26
3.2 Combustion Modeling	29
3.3 Finite Rate Chemistry	32
3.4 Governing Equations	34

4	Summary of Papers	37
4.1	Paper I	37
4.1.1	Motivation and Background	37
4.1.2	Work and Results	39
4.1.3	Comments	40
4.2	Paper II	40
4.2.1	Motivation and Background	40
4.2.2	Work and Results	41
4.2.3	Comments	41
4.3	Paper III	42
4.3.1	Motivation and Background	42
4.3.2	Work and Results	42
4.3.3	Comments	43
4.4	Paper IV	45
4.4.1	Motivation and Background	45
4.4.2	Work and Results	45
4.4.3	Comments	46
4.5	Paper V	46
4.5.1	Motivation and Background	46
4.5.2	Work and Results	46
4.5.3	Comments	46
5	Unpublished Results	49
5.1	PDE Configuration	49
5.2	Pulse Detonation Cycle	50
5.3	Test Case	51
5.4	Computational Domain	53
5.5	Numerical Method	54
5.6	Results	56
5.7	Fill Phase	57
6	Concluding Remarks	63
6.1	Future Work	64
	Bibliography	67
	A Preconditioning	75
	B Species Diffusive Flux Approximation	77
	C Hybrid LES/URANS	79
	Paper I	

Paper II

Paper III

Paper IV

Paper V

Chapter 1

Introduction

1.1 Motivation

CHEMICAL REACTIONS are nearly always accompanied either by an absorption or release of energy which manifests itself as heat. Heat released from chemical reactions in the burning process of fossil fuels has been the major source of energy for mankind since the industrialization era started. Today, despite all technical improvements and global efforts in exploiting other sources of energy such as solar, wind and nuclear energy, combustion of fossil fuels still accounts for more than 80% of the total energy consumption. The rapid growth of population together with the growth in average energy consumption per person has made it impossible to decrease the rate of consumption of fossil fuels in favor of other substitutes. It is unequivocally expected that fossil fuels will remain the main source of energy for domestic heating, power generation and transportation for at least a few decades to come. Therefore, combustion as one of humanity's oldest technologies will remain a key technology in the foreseeable future.

Unfortunately, heat is not the only product in the combustion of fossil fuels. Combustion always changes the chemical composition of the reactants and produces new molecules. Fossil fuels are hydrocarbon molecules which are made of carbon and hydrogen atoms. Ideally, in the complete combustion of hydrocarbons, the products are carbon dioxide CO_2 and water vapor H_2O . However, non-ideal and incomplete combustion process which always happens in practice not only produces heat, CO_2 and water but also unwanted pollutants in form of soot, carbon monoxide CO , nitrogen oxides NO_x , unburned hydrocarbons, etc. Carbon dioxide and water vapor belong to the family of greenhouse gases which are known to contribute to the global warming phenomenon. Moreover, carbon dioxide is involved in the process

of ocean acidification. While human activities does not significantly affect the concentration of water vapor in the atmosphere, except very locally, anthropogenic increase in carbon dioxide concentration has been noticeable. It is believed that the burning of fossil fuels is the main reason for the increase in tropospheric carbon dioxide concentration from 280ppm in pre-industrial times to 396ppm today. Unlike the long term effects of greenhouse gases, carbon monoxide and nitrogen oxides are poisonous and are known to be immediately dangerous for human life. Carbon monoxide is very toxic if inhaled and can be fatal. The nitrogen oxides can form nitric acids which are dangerous and can cause or worsen respiratory diseases.

One major contribution to the CO_2 production is the transport sector which is dominated by consumption of fossil fuels in different kinds of engines. Today, aviation accounts for about 2.5% of total anthropogenic CO_2 production. However, air transport is becoming more common and studies have shown that significant increase in air passenger traffic is expected in the future. Therefore, air transport will play a more prominent role in air pollution and global warming in the future.

The continuous need for energy makes it impossible to abandon fossil fuels, however the environmental impacts are real and significant. Therefore, global attempts such as Kyoto Protocol have been made to enforce different countries to reduce the level of their pollutants production, CO_2 in particular, in order to confront the problem of global warming. Moreover, national and international authorities are constantly posing more and more stringent regulations on the acceptable level of NO_x emissions for industry, specially automotive and gas turbine industry. The combustion technology needs to address these issues and continuous improvement is needed if these ever increasing demands on reduced emission levels are to be met in the future.

1.2 Background

Turbulent combustion happens in nearly all practical burner applications and is an engineering problem of high interest. Turbulence, even in non-reacting medium, is far from being fully understood and is usually referred as the most significant unsolved problem in classical physics. The exact manner in which combustion and turbulence affect each other is an unresolved problem which has inspired many researchers in the past decades. The general view is that turbulence and combustion enhance each other, however they both have a range of different length and time scales that can interact and change this simple picture. Under certain circumstances, turbulence can even cease

combustion and result in local extinction of the flame. Although there is a significant lack of knowledge in turbulent combustion context, the urgent need for solving engineering problems has led to some preliminary solutions called combustion models.

Computational Fluid Dynamics (CFD) is one primary tool in turbulent flow studies. Turbulence models have been used in CFD to simulate non-reacting turbulent flows. There are several methodologies in solving the fluid flow equations. In Direct Numerical Simulation (DNS) all the scales of the flow are resolved and the flow equations are solved without any modeling assumptions. In Reynolds Averaged Navier-Stokes models (RANS) the mean quantities are computed and the effects of the fluctuations are modeled. DNS simulations require large number of grid cells to resolve all the scales of the flow and are out of the scope of industrial use for decades. RANS simulations on the other hand are well within the computational capabilities of the day but can not address the unsteadiness and dynamics of the flow, specially reacting flows where the flow-flame interact at different scales and the flow field exhibits high levels of unsteadiness and instability. Large Eddy Simulation (LES) is an intermediate solution between DNS and RANS which resolves large and intermediate scales and only models small scales of the flow. The behavior of the small scales are believed to be universal and LES models theoretically do not suffer from lack of generality inherent in RANS models. The grid resolution in LES calculations specifies the range of scales which are resolved, therefore still large number of grid cells are needed for LES simulations compared to RANS models. Although LES was first proposed in 60s it is only in recent years that the growth in the power of computational facilities enables LES computations on a practical test case. In spite of this growth, LES simulations are still too slow to be performed on a single processor due to tremendous number of grid cells needed for resolving the intermediate scales of the flow. This necessitates the use of parallel computations on several processors. Message Passing Interface libraries (MPI) are ready-to-use functions and procedures in C++ and Fortran which are used for communication between several processors in a parallel environment. MPI is widely used for parallelization of numerical solvers for solving flow equations.

One natural way to study turbulent reacting flows is to incorporate models for turbulence-combustion interactions into the well known turbulence models. This has been done for RANS turbulence models before and many combustion models have been proposed. However, reacting flows are highly unsteady and the interactions of combustion scales with turbulence scales are not very well known. The flow structures

can corrugate the flame front and significantly affect the flame stabilization mechanism in practical applications. This makes it difficult to model the combustion phenomenon and to simulate the reacting flows with RANS models. The rapid growth of the computer powers in the recent years and the possibility of performing computations on several processors in parallel, have made the simulations using Large Eddy Simulation (LES) possible even for reacting flows. Some of the unsteady structures and flow-flame interactions are resolved in LES and the uncertainty of the combustion modeling is narrowed to the smallest scales of the flow. Nevertheless, combining LES with combustion models is a fairly new topic and there is still a vast variety of problems to be solved. The flow equations in LES are spatially filtered and the thickness of the flame front is less than the typical LES grid resolution which indicates that the whole reaction zone is filtered out and can not be resolved. This poses extra modeling problems in numerical simulations of reacting flows in LES. Numerical instabilities are another source of problem which need to be addressed when combustion models are incorporated into the flow equations; after all, numerical techniques need to be applied for solving the governing equations and combustion models should avoid adding extra difficulties.

There is a wide range of numerical methods and combustion models suggested for reacting flow studies and a proper test case is needed to evaluate the potential of these methods in predicting the flow field, flame position, flame stability and other characteristics of reacting flows. The test case should be well documented and easy to be modeled in numerical codes. It should also offer simple and well defined boundary conditions.

1.3 Low Swirl Burner

Production of carbon monoxide and nitrogen oxides are highly dependent on the operating temperature of the technical processes as shown in figure 1.1. The production of NO_x decreases with reduced flame temperatures while the production of CO increases.

In a stoichiometric fuel/air mixture the amount of oxygen is just enough to burn all the fuel while in a lean mixture there exist an excess amount of oxygen which not only helps to complete the burning process of all unburned/ill-burned products but also results in a lower flame temperature. Lean premixed combustion has increasingly gained interest in recent years as an approach toward low NO_x emissions. However, lean blow off limit and the tendency of the dynamic flame to become unstable present technical challenges. The Low swirl stabilized

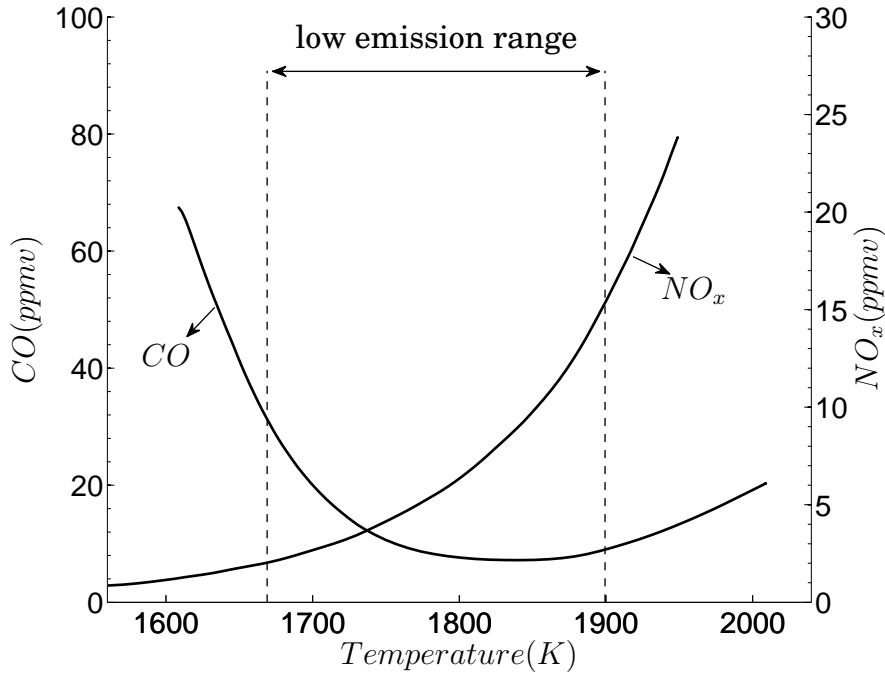


Figure 1.1: Temperature dependence of emissions for typical gas turbine combustion (Lefebvre (1999)).

combustion concept is a rather new and promising design to stabilize lean premixed flames close to their flammability limit. This enables the burner to work at lower temperatures, hence producing lower NO_x emissions (Cheng *et al.* (2000); Littlejohn *et al.* (2002); Johnson *et al.* (2005); Cheng *et al.* (2009)).

In view of the need for a test case for validation of numerical methods and combustion models, a low swirl burner similar to the design originally proposed by R. K. Cheng and co-workers (Chan *et al.* (1992); Bédard & Cheng (1995); Cheng *et al.* (2000)) was chosen and three identical burners were manufactured and installed at Lawrence Berkley National Laboratory (LBNL), Darmstadt University and Lund university (Petersson *et al.* (2007)). Since then this burner and its associated flame has been the subject of several experimental and numerical studies (Nogenmyr *et al.* (2007); Petersson *et al.* (2007); Nogenmyr *et al.* (2009, 2010); Day *et al.* (2012)). This low swirl burner has a simple design with few complicated components and can be relatively easily modeled in numerical solvers. However, the main problem in numerical simulation of this burner is the uncertainty in specifying the inlet boundary condition. It has been shown that the choice of the computational domain and the inlet boundary condition significantly affects the

results (Nogenmyr *et al.* (2010)). In order to make this flame a proper test case for LES studies the problem of uncertainty in specifying the inlet boundary should be solved so that the effects of numerical methods and combustion models on the results could be isolated from the effects imposed by the choice of the boundary conditions.

The first part of this thesis work was focused on investigating the effects and importance of the inlet boundary condition on prediction of the flow field and flame position as well as the flame dynamics in a low swirl burner and trying to solve the problem of inlet boundary uncertainty by providing proper and simple boundary conditions for numerical studies.

Lean premixed low swirl stabilized combustion concept is a promising technology to push the operating conditions of industrial burners close to lean blow-off limit. Hence, meeting the ever increasing demands on reducing NO_x emissions. Low swirl concept is proved to give very low emission levels while showing the capability of operating with different fuels under a rather wide range of operating conditions (Cheng *et al.* (2009); Littlejohn & Cheng (2007); Cheng *et al.* (2008, 2000)). In this context this test case is also of interest from a practical engineering point of view. The details of the geometry and working conditions of the burner are given in papers I, II and V.

1.4 Modern Aircraft Engines

Production of CO_2 in burning process of fossil fuels is inevitable and the only way to reduce its production is to decrease fuel consumption by increasing efficiency in engineering processes such as gas turbines. In spite of significant improvements in turbomachinery efficiency, the overall efficiency of modern aircraft engines are quite low. The room for efficiency improvement in the turbomachinery components is very limited and major improvements can only happen through innovative core designs. One of the main sources of loss in aircraft engines is the combustor. Conventional aircraft engines work with a Brayton cycle, or a modified Brayton cycle, in which the combustion happens at constant pressure. The constant pressure combustion is known to give low thermal efficiencies. The detonation mode of combustion is another option which has been considered for more than 70 years. In detonation a supersonic shock wave followed by a reaction zone is sustained which passes through the fuel/oxidizer mixture and rapidly burns it in a process close to a constant volume combustion. This mode of combustion, if applied in a jet engine frame, resembles the Humphrey cycle. The irreversibility, entropy generation, in this cycle is less than the

conventional constant pressure combustion which can yield a considerable increase in the overall engine efficiency. The thermodynamic cycle and potential efficiency benefits of Pulse Detonation Engine (PDE) concept has been the subject of a number of analytical and numerical studies (Paxson (2001); Kentfield (2002*a,b*); Wu *et al.* (2003); Goldmeer *et al.* (2008)). However, there are numerous physical and technical challenges needed to be addressed. The detonation is an intermittent process by nature, therefore any engine exploiting this phenomenon needs to work in a pulsating manner. In 2008 the first aircraft with a PDE was successfully launched. The engine was consisted of several pulse detonation tubes (PDT) that gave the necessary thrust for the flight. This demonstration showed that a PDE can be integrated into an aircraft frame without experiencing structural problems from the detonation waves. However, to fully exploit the detonation process in a practical aircraft these sets of tubes need to be integrated into an engine with the other components such as turbines and compressors (hybrid engine). The turbomachinery studies have always been focused on either steady conditions or short unsteady transients while the turbomachinery in a hybrid PDE is exposed to extreme intermittent unsteadiness. The effects of the unsteady flow on the turbine stage have been studied before (Rasheed & Tangirala (2004); Tangirala & Rasheed (2007); Zante & Turner (2007); Rouser *et al.* (2010)), however the compressor side has not been considered equally. The second part of this thesis has been focused on the integration of a set of pulse detonation tubes in the frame of a turbofan engine.

1.5 Thesis Objectives

Develop and modify an existing in-house LES solver in order to apply it for numerical studies of a low swirl stabilized flame. An appropriate outlet boundary condition was included and several turbulence-chemistry interaction models were implemented. The original solver was a sequential numerical code working on a single processor, therefore it was parallelized with the aid of MPI routines in order to speed up LES simulations.

Develop a proper combustion model for LSB studies which is easily incorporated into LES solvers and is capable of resolving the flame dynamics in the low swirl burner flow field.

Investigate the effects of the inlet boundary condition and to find the optimized computational domain and corresponding bound-

ary conditions in order to be used by other researchers for further LSB studies.

Investigate the flame stabilization mechanism in the low swirl burner flow field and understand the underlying flow-flame interactions phenomena which are responsible for flame stabilization.

Provide a simple combustion model for RANS which is capable of capturing the correct detonation wave properties.

Compare two alternative PDE configurations for their flexibility of working conditions by studying the unsteady phenomena at both compressor and turbine sides.

It should be mentioned that the time devoted to the second part of the thesis, the PDE part, was no more than 15% of the total time devoted to this thesis work.

Chapter 2

Combustion

COMBUSTION in a gaseous medium is classified as non-premixed, partially premixed and premixed combustion according to the mixing level of the fuel/oxidizer mixture prior to burning. Premixed combustion, which is the combustion mode considered throughout this thesis work, requires that the fuel and oxidizer are completely mixed before the combustion is allowed to take place. A premixed mixture of fuel and oxidizer is not reactive at low temperatures. However combustion can be initiated if a local heat source or other means of introducing radicals is applied in the mixture. This initiation of the burning process is called *ignition*. Once the mixture is ignited the burning process continues provided that the mixture is within the so called flammability limits. These flammability limits depend on the composition of the mixture. *Stoichiometric* condition happens when the amounts of fuel and oxidizer in the combustion compound are balanced so that after the combustion process is completed no fuel or oxidizer is left. If there exists an excess of fuel over oxidizer the mixture is called *rich* and if there is a deficit of fuel the mixture is called *lean*. The equivalence ratio of a mixture ϕ is defined as the ratio of the fuel-to-oxidizer mass fraction ratio to the stoichiometric fuel-to-oxidizer mass fraction ratio, equation 2.1. Most hydrocarbon fuels are flammable in the range of $0.5 < \phi < 1.5$.

$$\phi = \frac{Y_{\text{fuel}}/Y_{\text{oxidizer}}}{(Y_{\text{fuel}}/Y_{\text{oxidizer}})_{\text{stoichiometric}}} \quad (2.1)$$

2.1 Combustion Modes

When a flammable premixed fuel/oxidizer mixture is ignited the burning process can occur in three distinctive modes. In specific cases burning happens very rapidly and without any preferable direction. This is

the *explosion* mode of combustion. However, in most engineering processes the overall conditions lead to formation of a wave which passes through the mixture and burns it.

Figure 2.1 shows a tube filled with premixed fuel/oxidizer mixture. The velocities are shown both in the wave and unburned gas coordinate systems. If the tube is open at both ends the velocity of the wave is low and is controlled by transport processes, mainly simultaneous heat diffusion and diffusion of radicals. This results in a subsonic wave and the combustion mode is called *deflagration*; the wave is called flame, combustion wave or deflagration wave interchangeably. However, if the tube is closed at one end and the mixture is ignited at the same end the propagating wave undergoes a change from a subsonic wave to a supersonic wave. The burning process is not controlled by heat conduction or radical diffusion; rather, the shock wave passing through the unburned gas increases the temperature and pressure substantially and leads to rapid burning of the fuel. This supersonic front is called *detonation* wave and this combustion mode is called detonation. In both deflagration and detonation modes the propagating waves are sustained by the heat released from reactions.

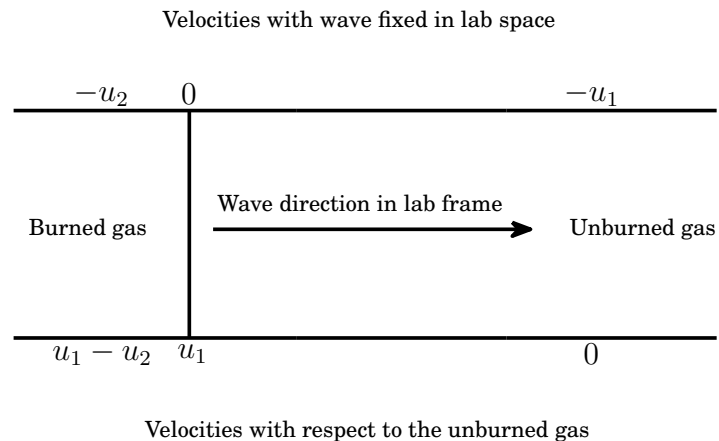


Figure 2.1: Tube case used for combustion mode analysis. Velocities in wave (top) and unburned gas (bottom) coordinates are shown.

Equations 2.2-2.6 represent the conservation of mass, momentum and energy together with equations of state for unburned and burned mixtures respectively, where subscript 1 denotes unburned and subscript 2 denotes burned mixture and q is the heat released from chemical reactions.

$$\rho_1 u_1 = \rho_2 u_2 \tag{2.2}$$

$$p_1 + \rho_1 u_1^2 = p_2 + \rho_2 u_2^2 \quad (2.3)$$

$$c_p T_1 + \frac{1}{2} u_1^2 + q = C_p T_2 + \frac{1}{2} u_2^2 \quad (2.4)$$

$$p_1 = \rho_1 R_1 T_1 \quad (2.5)$$

$$p_2 = \rho_2 R_2 T_2 \quad (2.6)$$

The unknowns in this set of equations are u_1, u_2, T_2, p_2 and ρ_2 . Equation 2.5 connects known variables and is redundant. Therefore, there are four equations and five unknowns, thus no eigenvalue solution exists for the problem and more information is needed to find a unique answer to the equations. With simple algebraic manipulation of the above equations the following relations are obtained. The assumptions of constant C_p (specific heat at constant pressure) and constant γ (specific heat ratio) are used in the following discussion.

$$\frac{\gamma}{\gamma - 1} \left(\frac{p_2}{\rho_2} - \frac{p_1}{\rho_1} \right) - \frac{1}{2} (p_2 - p_1) \left(\frac{1}{\rho_1} + \frac{1}{\rho_2} \right) = q \quad (2.7)$$

$$\gamma M_1^2 = \frac{\frac{p_2}{\rho_2} - 1}{1 - \frac{(\frac{p_2}{\rho_2})}{(\frac{p_1}{\rho_1})}} \quad (2.8)$$

$$\gamma M_2^2 = \frac{1 - \frac{p_1}{p_2}}{\frac{(\frac{p_1}{\rho_1})}{(\frac{p_2}{\rho_2})} - 1} \quad (2.9)$$

Equation 2.7 is called *Hugoniot* equation and relates the unknown variables on the burned side, p_2 and $\frac{1}{\rho_2}$, to the corresponding known variables on the unburned side. This equation gives a family of solutions for each specified heat release q . The case of $q = 0$ corresponds to a shock wave with no combustion, heat addition, and passes through the initial unburned condition p_1 and $\frac{1}{\rho_1}$. Figure 2.2 shows two such Hugoniot curves for an arbitrary q and for $q = 0$. Point *A* corresponds to the initial condition. The Hugoniot curve is hyperbolic and there are two tangent lines to it which pass through point *A*. These two lines together with the horizontal and vertical lines corresponding to initial pressure and density divide the Hugoniot curve into five distinct regions shown by roman numerals I-V in figure 2.2. Region V is characterized by $p_2 > p_1$ and $\frac{1}{\rho_2} > \frac{1}{\rho_1}$ which gives $M_1^2 < 0$ from equation 2.8. Therefore, this region does not represent physical solutions and is

directly ruled out. The discussion presented here can be found in more details in Glassman (1996).

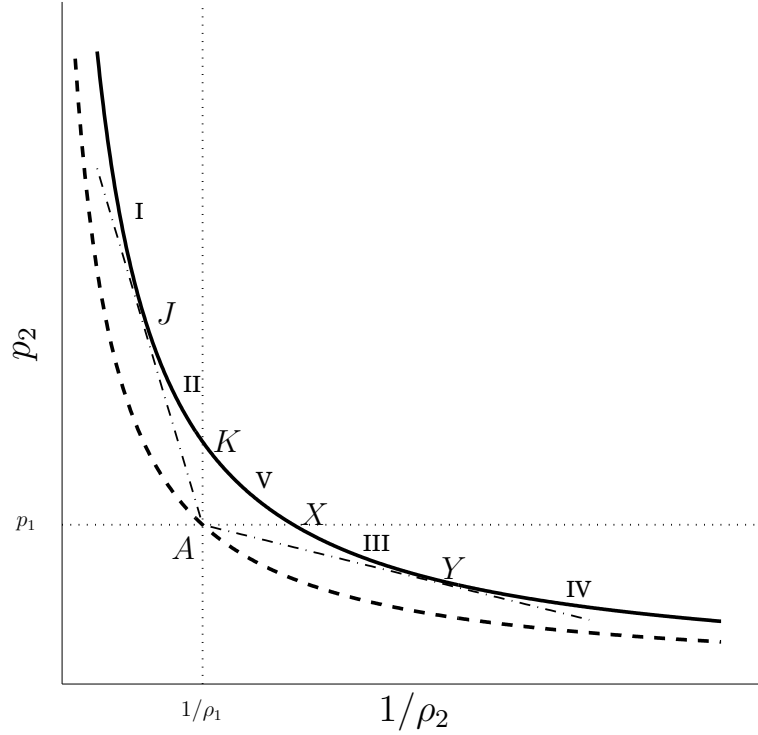


Figure 2.2: Hugoniot curves for $q = 0$, dashed line, and an arbitrary q , solid line.

2.2 Detonation

Examination of equation 2.8 reveals the characters of M_1 in regions I and II. In these regions p_2 is significantly larger than p_1 and $\frac{1}{\rho_2}$ is smaller than $\frac{1}{\rho_1}$. Consequently, the right hand side of equation 2.8 is much larger than 1 and certainly larger than 1.4 which is a conservative value for γ . Therefore, $M_1 > 1$ and these regions define a supersonic compression wave and are together called detonation region. It can be shown that the flow at tangent point J is sonic in the coordinate system attached to the wave front, equations 2.10.

$$u_{2,J} = c_{2,J} \quad M_{2,J} = 1 \quad (2.10)$$

This implies that the waves corresponding to these regions can be further categorized as below.

- Region I: Strong detonation since $p_2 > p_J$ (supersonic flow to subsonic)
- Region II: Weak detonation since $p_2 < p_J$ (supersonic flow to supersonic)

There is no condition by which strong detonation can be ruled out, however it is argued by Chapman and Jouguet that the results in this region are unstable everywhere except at J . Furthermore, assuming a specific structure for the detonation wave as a shock wave followed by a reaction zone, which will be shortly discussed as ZND model, rules out region II. Consequently, the only possible solution in the detonation side is point J which is called the Chapman-Jouguet plane. Strong detonation can only happen as transient modes and would quickly break down and fall into Chapman-Jouguet condition. The detonation wave is a compression wave and the burned gases at Chapman-Jouguet plane follow the wave front at the speed of sound, as indicated by the unity of Mach number at Chapman-Jouguet plane.

The fact that the detonation waves should fall into a single point J on the Hugoniot curve suggests that an eigenvalue solution to equations 2.2-2.6 does exist in this region. Therefore all the unknowns in these equations can be uniquely determined without any further assumptions and post-detonation conditions are uniquely determined.

2.2.1 ZND Structure of the Detonation Wave

Zeldovich, von Neumann and Döring independently arrived at a theory for the structure of the detonation wave. The ZND theory states that the detonation wave is a planar shock wave followed by a reaction zone. The shock wave moves at the detonation velocity and increases the pressure and temperature of the unburned mixture behind it. Chemical reactions are exponential functions of the temperature; in case the temperature right behind the shock is not high enough to rapidly consume all the fuel a slowly burning region, induction zone, is formed behind the shock and combustion progresses and temperature gradually increases to values that rapidly burn all the remaining fuel in a very short distance. At the same time the temperature increases and pressure decreases until they match the the Chapman-Jouguet conditions.

ZND structure of the detonation wave is shown in figure 2.3. The shock wave increases the pressure and temperature from point 1 to 1'.

The induction zone immediately follows and is characterized by very small changes in mixture properties. Chapman-Jouguet plane is at point 2 which is preceded by a very thin reaction zone. The kinetics and mechanism of reactions together with the temperature level behind the shock wave give the spatial and temporal separation of the shock front and Chapman-Jouguet plane. The induction zone could be very thin if the temperature behind the shock is high enough to immediately burn all the fuel.

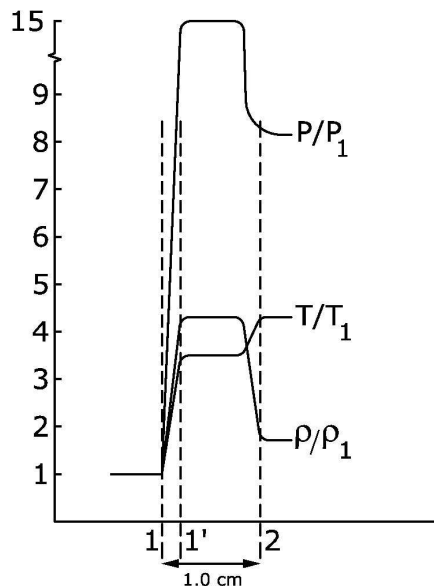


Figure 2.3: Structure of the detonation front according to ZND model. The pressure, temperature and density ratios correspond to the initial conditions presented in paper III. The width of the induction zone is typical of detonation waves at low initial pressures and does not correspond to the initial conditions in paper III.

No presumed wave structure was needed to compute the detonation velocity and Chapman-Jouguet conditions, however wave structures of ZND form were used to rule out the weak detonation region in the discussion above. At the end it is worth to mention that ZND concept considers the detonation wave to be one-dimensional while there is evidence that self-sustained detonation waves have three-dimensional cellular structure.

2.3 Deflagration

Characteristics of M_1 in regions III and VI can be studied by examining equation 2.8 in the same way as what was done for regions I and II. In these regions p_2 is smaller than p_1 and $\frac{1}{\rho_2}$ is larger than $\frac{1}{\rho_1}$. Consequently, the right hand side of equation 2.8 is smaller than 1. Therefore, $M_1 < 1$ and these regions define a subsonic wave and are together called deflagration region. It can be shown that the flow at tangent point Y is also sonic in the coordinate system attached to the wave front, equations 2.11, and deflagration region can be further categorized as below.

- Region III: Weak deflagration since $p_2 > p_Y$ (subsonic flow to subsonic)
- Region IV: Strong deflagration since $p_2 < p_Y$ and $\frac{1}{\rho_2} > \frac{1}{\rho_Y}$ (subsonic flow to supersonic)

$$u_{2,Y} = c_{2,Y} \quad , \quad M_{2,Y} = 1 \quad (2.11)$$

$\frac{1}{\rho_2} > \frac{1}{\rho_Y}$ in region IV, therefore velocities are greater than $u_{2,Y}$ due to continuity while the speed of sound is about equal to the speed of sound at Y . Therefore, as stated above, the flow is supersonic behind the shock in this region. This indicates that the flow in a constant area duct should pass the sonic point by heat addition which is impossible and region IV is ruled out.

Region III can not be ruled out and the whole region contains physical solutions. This region corresponds to the deflagration mode of combustion and encompasses the laminar flame family of solutions. In order to uniquely specify the deflagration velocity for a set of initial conditions another equation is needed. This equation comes from the examination of the structure of the deflagration wave and deals with the rate of chemical reactions or, more specifically, the rate of heat release. In other words, treating the combustion wave as a discontinuity does not yield any unique answer and the structure of the flame needs to be resolved for this purpose.

2.3.1 Premixed Flame Structure

Structure of a typical premixed flame is shown in figure 2.4. It consists of three separate zones, a preheat zone, a reaction zone also called the inner layer and a recombination zone also referred as the oxidation

layer. The preheat zone is chemically inert and the changes in concentration of species and the temperature variations are caused by diffusion from downstream. In the inner layer the fuel is completely consumed and temperature increases. This layer is chemically active and is responsible for keeping the reactions alive. The oxidation layer falls into the burned gas or post-flame zone. Although the recombination reactions are very exothermic here, the concentration of recombining radicals are so low that the temperature profile does not change significantly. The characteristics of a premixed flame and the composition changes across it are determined by the competition between the convective flow of the unburned gases toward the flame and the diffusion of heat and radicals from the high-temperature reaction zone against the convective flow into the preheat region.

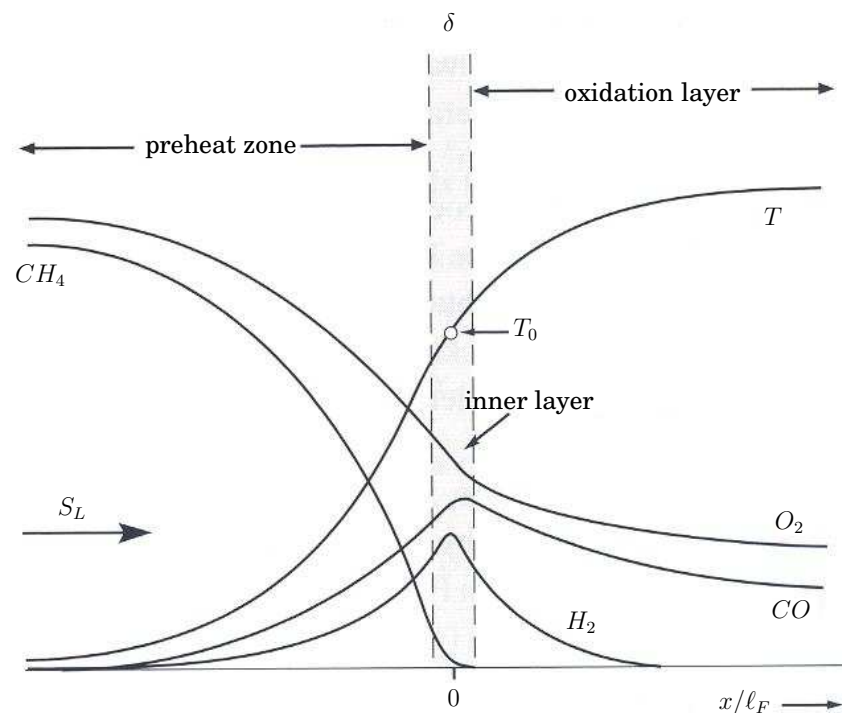


Figure 2.4: Structure of a premixed methane flame.

2.3.2 Laminar Flame Speed

Flame velocity or laminar flame speed, S_L , is the velocity at which unburned gases move through the combustion wave in the direction normal to the wave surface. In other words, it is the velocity at which

the flame front propagates normal to itself and relative to the flow into the unburned mixture. It is represented by u_1 in figure 2.1. Laminar flame speed is a thermo-chemical transport property that depends on fuel/oxidizer mixture, the equivalence ratio, temperature and pressure. Any exact solution of laminar flame propagation must make use of basic equations of fluid dynamics modified to account for the liberation and conduction of heat and for changes of chemical species within the reaction zones. It is possible to solve these equations numerically using detailed reaction mechanisms and molecular transport properties. These are called the comprehensive models for laminar flame calculations. However, by using certain physical assumptions and mathematical techniques these set of complicated equations can be simplified and analytically easy to handle. Although computer codes can simply calculate the laminar flame speed and flame thickness from these detailed equations, combustion modeling can still benefit from simple analytical approaches as they provide simplified relations.

Thermal theories are the simplest analytical theories in laminar flame calculations which assume only the heat diffusion in resolving the flame front structure. The theory of Mallard and Le Chatelier falls into this group of theories. By assuming an ignition temperature T_L , below which no reactions occur, this theory gives the laminar flame speed and the reaction zone thickness according to equations 2.12 in which S_L , δ_L , D and \bar{W} are the laminar flame speed, flame thickness, heat diffusivity and average reaction rate respectively.

$$s_L \propto \sqrt{D\bar{W}} \quad \delta_L \propto \frac{D}{s_L} \quad (2.12)$$

Diffusion theories further consider the diffusion of molecules. However, since these theories assume that the flame propagation is fundamentally a thermal mechanism they do not consider the diffusion of atoms and radicals. The theory of Zeldovich, Frank-Kamenetskii and Semenov belongs to this category of theories. The threshold temperature considered in the Mallard Le Chatelier theory is also applied here, however it is assumed to be very close to the flame equilibrium temperature and is eliminated from the mathematical development. This theory gives the same two proportionality relations given in equation 2.12.

2.4 Turbulent Combustion

Combustion requires that the fuel and oxidizer are mixed at molecular level to have the chance to collide and react. Turbulence increases

the mixing process and thereby enhances combustion. On the other hand, combustion process releases heat and generates flow instabilities which then enhance the transition to turbulence. Therefore, combustion nearly always takes place within a turbulent rather than a laminar flow field in technical processes. The turbulent mixing process dominates the molecular mixing required for combustion. The general view in turbulent mixing is that once a range of different eddies have developed, strain and shear at the interface of the eddies enhance mixing. During the eddy break up process and the formation of smaller eddies, strain and shear increase which steepen the concentration gradients at the interface between reactants and enhance the molecular inter-diffusion. Chemical reactions consume the fuel at the interface and steepen the gradients more. The way in which the combustion changes this picture and modifies the turbulent mixing process is not yet clear.

Reaction rates are usually of exponential nature and chemical reactions are nearly always fast compared to all turbulent time scales. These active reactions concentrate in thin layers which are typically thinner than the Kolmogorov length scale. These thin layers can not exert any feedback on the flow except for density changes. If these layers extinguish due to any reason, the chemistry becomes very slow. In both fast and slow chemistry situations, time and length scales of combustion and those of turbulence in the inertial sub-range are separated, hence the mixing process can be explained by classical mixing theories. This *scale separation* makes the mixing process in the inertial sub-range independent of chemistry and simplifies the combustion modeling (Peters (2000)).

2.5 Turbulent Flame Speed

The mass consumption rate per unit area in a premixed laminar flame is $\rho_u S_L$ where ρ_u is the unburned gas density. The consumption rate increases in a turbulent flow field and a corresponding turbulent flame speed S_T can be defined to relate the consumption rate and density. The turbulent flame speed is an averaged property and depends on the characteristics of the turbulent flow field and the flame stabilization mechanism. If the turbulent length scales are significantly larger than the flame thickness, as in a low intensity large scale turbulence, one can assume the flame front as a corrugated laminar flame which has an effective area larger than a simple planar laminar flame. The ratio of turbulent to laminar flame speeds would then be simply the ratio of the corresponding effective flame areas. Based on calculating the

increase in flame area in a large scale low intensity turbulent flow field, Damköhler suggested equation 2.13 for the turbulent flame speed in which U' is the turbulent intensity ahead of the flame front.

$$S_T = S_L + U' \quad (2.13)$$

Other approaches for calculating the increase in flame surface in large scale low intensity turbulence have been tried. The works of Clavin-Williams (Calvin & Williams (1979)) and Schelkin (Schelkin (1947)) resulted in correlations given by equations 2.14 and 2.15 respectively.

$$\frac{S_T}{S_L} \sim \left\{ 1 + \left[\frac{\overline{(U')^2}}{S_L} \right] \right\}^{1/2} \quad (2.14)$$

$$\frac{S_T}{S_L} = [1 + (2U'/S_L)]^{1/2} \quad (2.15)$$

There are a number of other turbulent flame speed correlations, e.g. Zimont (Zimont & Lipatnikov (1995)), Gülder (Gülder (1990)), Peters (Peters (1999)), etc. These models are usually in the form of equation 2.16 in which f is a functional of the hydrodynamical and physico-chemical parameters expressed via the Reynolds, $Re = \frac{u_t l_t}{\nu}$, Damköhler, $Da = \frac{\tau_t}{\tau_c}$, and Prandtl, $Pr = \frac{\nu}{\alpha}$ numbers.

$$\frac{S_T}{S_L} = 1 + f(Re, Da, Pr) \quad (2.16)$$

Most of flame wrinkling and corrugation is resolved in LES and the turbulent flame speed calculation is narrowed to the increase of the flame surface due to subgrid corrugation of the flame. This subgrid-scale turbulent flame speed is often assumed to be related to subgrid scale turbulence level u'_{sgs} according to equation 2.17 where α and n are constants.

$$\frac{S_T}{S_L} = 1 + \alpha \left(\frac{u'_{sgs}}{S_L} \right)^n \quad (2.17)$$

A complete discussion about turbulent flame speed is given in Lipatnikov & Chomiak (2002).

2.6 Reduced Chemistry

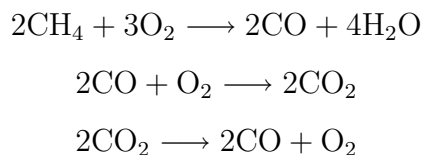
There is a large number of reactions and active species, including radicals, present in the combustion process of even the simplest fuels. This is not a particular problem when simple one-dimensional equations are

solved, for example in laminar flame speed calculations. However, it is not economical to solve this huge set of equations in three dimensions. Moreover, the reaction rates have an exponential dependence on temperature in nature, thus the reaction rates are very sensitive to temperature changes. Therefore, at certain temperatures some of the reactions might be very fast compared to the others which results in the stiffness problem in solving the set of equations. One solution to this problem is to reduce the number of equations by making equilibrium assumption for faster reactions and modifying the others to account for this assumption. This results in a reduced reaction mechanism which still represents the main characteristics of the original mechanism.

A further step in reducing the number of reactions and active species is to replace the detailed mechanism by a set of new reactions which do not even actually exist in nature but are an integral form of several elementary reactions. It is reasonable to reduce the number of reactions so that it is possible to incorporate them in three-dimensional calculations. The reaction rates in these global reactions are usually given by the so called Arrhenius expressions given in equation 2.18 in which RR , A , T , n and E_a are reaction rate, pre-exponential factor, temperature, a constant and activation energy respectively. The coefficients in these Arrhenius expressions are specified in a way that certain properties of the detailed mechanism such as flame temperature, CO concentration or laminar flame speed are reproduced by the reduced global mechanism.

$$RR = AT^n e^{-E_a/T} \quad (2.18)$$

One such global mechanism for methane/air mixture is given in Meredith & Black (2006). The detailed mechanism is reduced to only three reactions involving five species and the reaction rates are given by equation 2.19. This mechanism is originally optimized for temperature and CO concentration predictions at atmospheric conditions and for a limited range of equivalence ratios.



$$\dot{w}_i = A_i T^{\beta_i} e^{-E_{a_i}/RT} \prod_{j=1}^{N_j} [X_j]^{a_{i,j}} \quad (2.19)$$

Figure 2.5 compares the flame structure for a lean premixed mixture of methane/air at $\phi = 0.62$ calculated from both the detailed GRI

mechanism (GRI-Mech) and Meredith global mechanism. The flame calculations are performed using comprehensive theories. Not shown in this figure is the laminar flame speed which was computed to be about $S_L = 0.125$ for GRI-Mech and about $S_L = 0.13$ for Meredith mechanism. The global mechanism gives surprisingly comparable results to the detailed mechanism at this specific equivalence ratio, however at larger equivalence ratios it starts to significantly deviate from GRI mechanism.

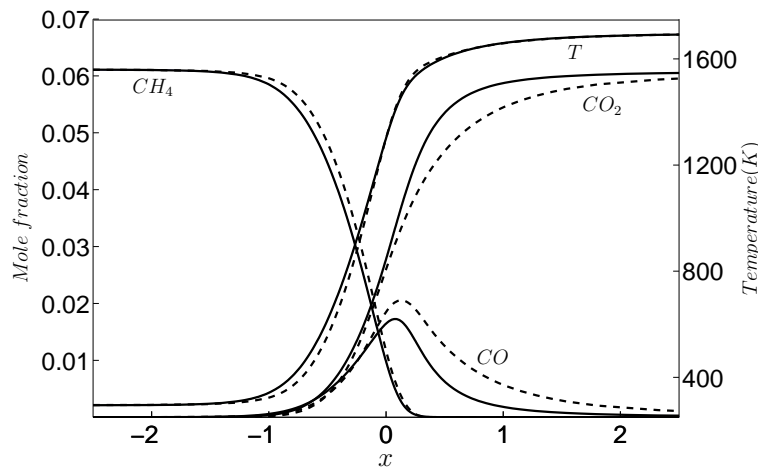


Figure 2.5: Structure of lean premixed methane/air flame at $\phi = 0.62$ computed by comprehensive laminar flame theories for GRI detailed mechanism, solid lines, and Meredith three step global reaction mechanism, dashed lines.

2.7 Flame Stabilization

Typical working velocities in practical combustion devices in which high volumetric heat release rates are needed exceed not only the laminar but also the turbulent flame speed of hydrocarbon fuel mixtures. This makes it impossible to stabilize a flame unless some other means are used. It is possible to achieve a continuous ignition of fresh mixture by adding a pilot flame in the flow, however these pilot flames are added inconvenience to the system and are usually not used. In practice, stabilization is accomplished by causing some of the hot combustion products to recirculate, thereby continuously igniting the fresh mixture coming from upstream. The recirculation can be achieved by several means such as introducing a solid obstacle as a flame holder (bluff-body stabilization), by directing part of the flow in the direction

opposed to the main flow direction, by introducing a step in the wall enclosure, by exploiting the vortex break down and the subsequent flow recirculation of a diverging swirling jet (swirl stabilization), etc.

Figure 2.6 shows the swirl stabilization concept. The swirling jet anatomy shown here corresponds to the low swirl stabilization mode in which only part of the flow gains the swirl velocity component. In a conventional high swirl stabilized flame the axial core region in figure 2.6 is eliminated and the whole flow is given a swirl velocity component.

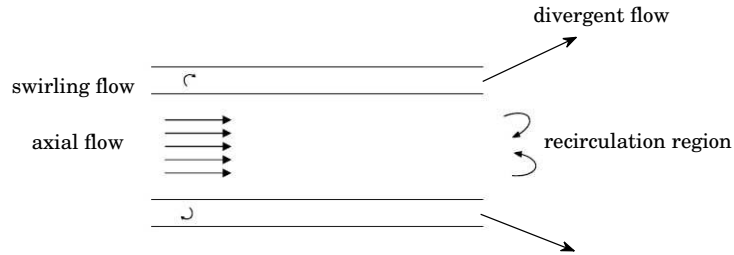


Figure 2.6: Principles of swirl flame stabilization.

2.8 Turbulent Combustion Regimes

Structure of a premixed flame was shown in figure 2.4 in which the x coordinate was scaled with a flame thickness ℓ_F . The flame thickness is a result of diffusive phenomena characterized by a diffusivity D . It is convenient for scaling purposes to assume equal diffusivities for all reacting scalars and to assume a Schmidt number of unity $Sc = \frac{\nu}{D}$. The flame velocity scale is the laminar flame speed S_L and addition of the diffusivity D as a scale gives the flame length scale (flame thickness) and the flame time scale, equation 2.20.

$$\ell_F = \frac{D}{S_L} = \frac{\nu}{S_L}, t_F = \frac{D}{S_L^2} = \frac{\nu}{S_L^2} \quad (2.20)$$

The thickness of the preheat zone, inner layer and oxidation layer are typically of the order of ℓ_F , $0.1\ell_F$ and $0.3\ell_F$ respectively (Peters (2000)). Comparing the scales of the flame with that of the turbulence leads to classification of the turbulent premixed flames into several regimes. Two sets of turbulent scales are considered, large integral

scales (ℓ , v' and ℓ/v') and small Kolmogorov scales defined in equation 2.21.

$$\eta = \left(\frac{\nu^3}{\varepsilon}\right)^{1/4}, t_\eta = \left(\frac{\nu}{\varepsilon}\right)^{1/2}, v_\eta = (\nu\varepsilon)^{1/4} \quad (2.21)$$

Based on these scales a turbulent Reynolds number, a Damköhler number and a Karlovitz number are defined in equations 2.22, 2.23 and 2.24 respectively.

$$Re = \frac{v'\ell}{D} = \frac{v'\ell}{\ell_F S_L} \quad (2.22)$$

$$Da = \frac{\ell/v'}{\ell_F/S_L} \quad (2.23)$$

$$Ka = \frac{t_F}{t_\eta} = \frac{\ell_F^2}{\eta^2} = \frac{v_\eta^2}{S_L^2} \quad (2.24)$$

Another relevant Karlovitz number can be defined based on the inner layer thickness as the proper flame length scale, equation 2.25.

$$Ka_\delta = \frac{\ell_\delta^2}{\eta^2} = \delta^2 Ka \sim 0.01 Ka \quad (2.25)$$

Figure 2.7 illustrates the classification of premixed flames into five regimes. Laminar flames happen at Reynolds numbers less than unity. All the other regimes are within the turbulent premixed category. Wrinkled flamelets regime is characterized by $Re > 1$, $Ka < 1$ and $Da > 1$ and in terms of the scales by $\ell/\ell_F > 1$ and $v'/S_L < 1$. This indicates that the turbulent intensity is smaller than the flame speed and laminar flame propagation dominates the flame front corrugation. Large scales of turbulence are larger than the flame thickness and can not interact with the internal structure of the flame. The small scales of the flame are faster than the small scales of turbulence and are not affected. In this regime turbulence can not interfere with the flame.

In the corrugated flamelets regime the turbulent velocity scale overcomes the laminar flame speed and leads to corrugation of the flame front. In the thin reaction zones regime $Ka > 1$ hence $\ell_F > \eta$ and the turbulent small scales can penetrate into the reactive-diffusive flame structure and distort it but they are still larger than the inner layer thickness. In the broken reaction zones regime $Ka_\delta > 1$ and the small scales of turbulence can enter the inner layer and affect the structure of it possibly leading to local quenching of the flame.

Most practical turbulent flames are either in corrugated flamelets or thin reaction zones regimes. The flame in the core region of the low

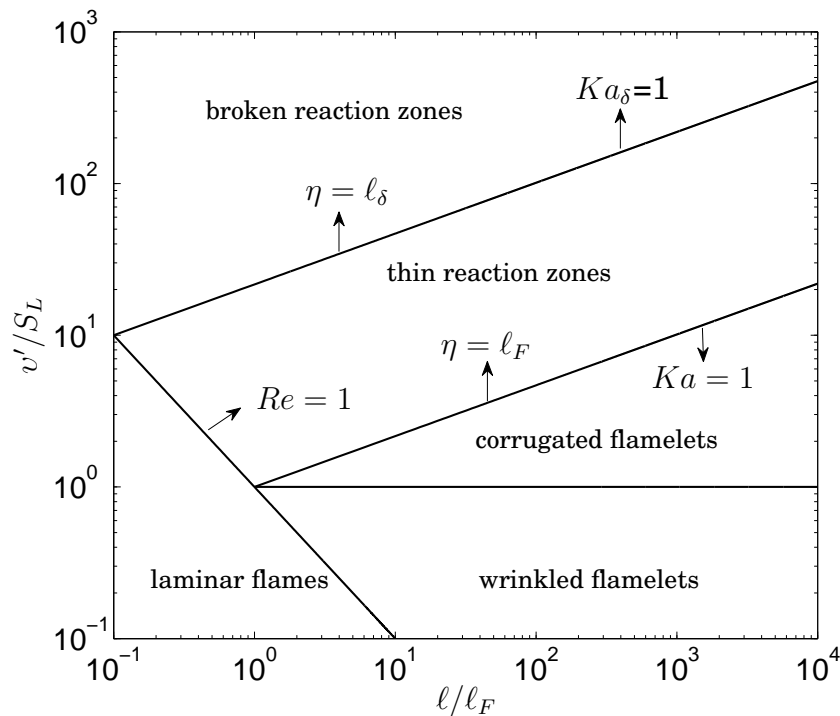


Figure 2.7: Turbulent premixed combustion regimes diagram (Peters (2000)).

swirl burner is in the border of corrugated flamelets and thin reaction zones regimes. However, the turbulent scales are smaller in the shear layer and flame scales are larger due to dilution of the mixture by mixing with co-flow air. The flame in the shear layer is in the border of thin reaction zones and broken reaction zones regimes. Mixing process can dilute the mixture to equivalence ratios below the flammability limit which results in local extinction of the flame.

Chapter 3

Methodology

TWO PREMIXED reacting flows are studied in the present work: the flow in a pulse detonation engine and the flow in a low swirl burner. Reactive nature of these flows implies that they both undergo density and composition changes. However, these two flows are very different in nature. Moreover, the objectives of these two studies are different which implies that the same numerical method might not suit both studies. The main numerical tool used in this work is a compressible computational fluid dynamics (compressible CFD) code developed by Eriksson (1995). This code solves the Navier-Stokes, $k - \varepsilon$ turbulence model and species transport equations on a block structured non-orthogonal curvilinear boundary-fitted computational grid using standard cell-centered finite volume method. The diffusive flux is approximated with a locally centered second order scheme while a low dissipation third order accurate characteristic upwind scheme gives the convective flux. The equations are integrated in time using a three-stage Runge-Kutta time stepping method. The details of the numerical schemes can be found in Eriksson (1995) and Andersson (2005).

The range of velocities in the low swirl burner flow field is well below the compressibility limit, $M \ll 0.3$, density changes are due to temperature variations and the flow is incompressible. The combustion is at low speed, deflagration mode, and happens in a turbulent flow field which implies that the structure of the flame front and turbulence-chemistry interactions are important features. The flow and the flame exhibit a wide range of structures which presumably contribute to the flame stabilization mechanism. RANS turbulence models do not seem to be adequate to resolve the flow-flame structures, thus LES methods were chosen for LSB studies. Preconditioning concept was used to economically solve this incompressible flow with a standard compressible flow solver. The details of the preconditioning technique are presented in appendix A. The Meredith three-step global reaction mecha-

nism gives the reaction rates which are then corrected for chemistry-turbulence interactions through a finite rate chemistry upwind thickened flame combustion model. Combustion happens far from the walls and is dominated by the larger flow structures, therefore walls do not play a significant role in this flow. Thus, the walls are not resolved and are treated through wall functions.

On the other hand, the velocities in the PDE flow field are well above compressibility limits and density changes are primarily due to pressure variations. The combustion is in detonation mode and the exact structure of the flame front and its interactions with turbulence are not important. Two-dimensional URANS with realizable standard $k - \varepsilon$ turbulence model with wall functions were used for PDE simulations. Combustion modeling does not need to address any interactions with the flow. The aim of the combustion model is to assure that detonation happens under certain circumstances and results in the correct post-combustion conditions. Burning is modeled at a finite rate given by an Arrhenius expression in a single step reaction mechanism. The constants in this Arrhenius expression are tuned to assure the onset of detonation.

3.1 Multi-Species Reacting Systems

The governing equations of Newtonian fluid flow which are the compressible form of continuity, momentum and energy conservation equations are given in equations 3.1-3.3 in which $e_0 = e + \frac{1}{2}u_m u_m$ is the total internal energy, q is the diffusive heat flux and τ_{ij} is the viscous stress tensor. The viscous stress tensor is given by equation 3.4 where S_{ij} , equation 3.5, is the strain-rate tensor. Effects of radiation and body forces are neglected.

$$\frac{\partial \rho}{\partial t} + \frac{\partial(\rho u_j)}{\partial x_j} = 0 \quad (3.1)$$

$$\frac{\partial(\rho u_i)}{\partial t} + \frac{\partial(\rho u_j u_i)}{\partial x_j} = -\frac{\partial p}{\partial x_i} + \frac{\partial \tau_{ij}}{\partial x_j} \quad (3.2)$$

$$\frac{\partial(\rho e_0)}{\partial t} + \frac{\partial(\rho u_j e_0)}{\partial x_j} = -\frac{\partial(u_j p)}{\partial x_j} + \frac{\partial(u_i \tau_{ij})}{\partial x_j} - \frac{\partial q_j}{\partial x_j} \quad (3.3)$$

$$\tau_{ij} = \mu(2S_{ij} - \frac{2}{3}S_{mm}\delta_{ij}) \quad (3.4)$$

$$S_{ij} = \frac{1}{2}\left(\frac{\partial u_i}{\partial x_j} + \frac{\partial u_j}{\partial x_i}\right) \quad (3.5)$$

In case of a non-reacting single species fluid motion these equations can be closed by an equation of state which relates the thermodynamic properties of the fluid. The perfect gas assumption, equation 3.6, is often valid as the equation of state for gases.

$$p = \rho RT \quad (3.6)$$

Reacting flows are multi-species systems which undergo composition changes through chemical reactions. It is possible to consider separate conservation equations for individual species. However, it is more convenient to consider only one set of conservation equations for the mixture of species. In this work the mixture and all the species involved are assumed to be thermally perfect gases. Therefore, equation 3.6 also holds for the mixture in which $R = \sum_{n=1}^N Y^{(n)} R^{(n)}$ and $R^{(n)}$ are the mixture and species n gas constants respectively. If one further assumes that the mixture is in vibrational equilibrium then internal energy and enthalpy of the mixture are functions of the composition and temperature only (equation 3.7 in which the internal energy and enthalpy of species are functions of temperature only).

$$e = \sum_{n=1}^N Y^{(n)} e^{(n)}, h = \sum_{n=1}^N Y^{(n)} h^{(n)} \quad (3.7)$$

These individual internal energies and enthalpies are furthermore assumed to be absolute quantities, that is they are assumed to contain the heat of formation H_f . This is important in the case of chemical reactions with heat release. In real gases the temperature dependence in equation 3.7 is non-linear, however in many cases linearized relations, as the best linear fits in the range of working temperatures, are very good approximations. The following linear relations for individual species are considered in this work.

$$e^{(n)} = H_f^{(n)} + C_v^{(n)} T, h^{(n)} = H_f^{(n)} + C_p^{(n)} T, C_p^{(n)} = C_v^{(n)} + R^{(n)} \quad (3.8)$$

From the assumption above the following auxiliary relations for the mixture are obtained.

$$e = H_f + C_v T, h = H_f + C_p T, h = e + \frac{p}{\rho} \quad (3.9)$$

where

$$H_f = \sum_{n=1}^N Y^{(n)} H_f^{(n)}, C_v = \sum_{n=1}^N Y^{(n)} C_v^{(n)}, C_p = \sum_{n=1}^N Y^{(n)} C_p^{(n)}, C_p = C_v + R \quad (3.10)$$

The composition of the mixture is needed in order to calculate the gas properties of the mixture. The transport equations of species, equation 3.11, can be used to find the composition of the mixture $Y^{(m)}$.

$$\frac{\partial(\rho Y^{(m)})}{\partial t} + \frac{\partial(\rho u_j Y^{(m)})}{\partial x_j} = -\frac{\partial J_j^{(m)}}{\partial x_j} + S^{(m)} \quad (3.11)$$

where $Y^{(m)}$, $J^{(m)}$ and $S^{(m)}$ are the species m mass fraction, diffusion flux, and chemical source respectively.

The chemical source term $S^{(m)}$ is determined by the reaction mechanism (often through Arrhenius expressions). The diffusion flux $J^{(m)}$ is related to the diffusion velocity $\vec{V}^{(m)}$ and partial density $\rho^{(m)}$ according to

$$J^{(m)} = \rho^{(m)} \vec{V}^{(m)} = \rho Y^{(m)} \vec{V}^{(m)} \quad (3.12)$$

The diffusion velocity of the species m is the velocity of species m relative to the mass weighted velocity of the mixture, equation 3.13, and can be determined by solving the set of equations 3.14 where $X^{(m)}$ denotes mole fraction of species m and $D^{(mn)}$ is the binary diffusion coefficient (Kuo (2005)). Body forces and Dufour effects are neglected.

$$\vec{V}^m = v^{(m)} - \vec{v} \quad (3.13)$$

$$\nabla X^{(m)} = \sum_{n=1}^N \frac{X^{(m)} X^{(n)}}{D^{(mn)}} (\vec{V}^{(n)} - \vec{V}^{(m)}) + (Y^{(m)} - X^{(m)}) \frac{\nabla p}{p}, m = 1, 2, \dots, N \quad (3.14)$$

In a single-species system the diffusion heat flux is due to temperature gradient only and is usually modeled by Fourier's heat law, $q_j = -\lambda \frac{\partial T}{\partial x_j}$. However, the diffusion velocities of species in a multi-species system are not equal and another term is added to the diffusion heat flux to compensate for the excess/deficit of velocity of species m relative to the velocity of the mixture, equation 3.15.

$$q_j = -\lambda \frac{\partial T}{\partial x_j} + \sum_{n=1}^N J_j^{(n)} h^{(n)} = -\lambda \frac{\partial T}{\partial x_j} + \sum_{n=1}^N \rho Y^{(n)} V_j^{(n)} h^{(n)} \quad (3.15)$$

The set of equations 3.1-3.3 can be closed by N equations of state corresponding to the species in the system. The equations presented in this section govern the motion of a gaseous mixture whose properties are mass weighted averages of corresponding species properties. It

should be mentioned that only $N - 1$ species transport equations are really needed and the last equation is made redundant by the following consistency equations.

$$\sum_{n=1}^N Y^{(n)} = 1, \sum_{n=1}^N J_j^{(n)} = 0, \sum_{n=1}^N S^{(n)} = 0, \sum_{n=1}^N Y^{(n)} \vec{V}^{(n)} = 0 \quad (3.16)$$

One major simplification to the above governing equations is to approximate the species diffusion velocity using Fick's law

$$Y^{(m)} \vec{V}^{(m)} = -D^{(m)} \nabla Y^{(m)} \quad (3.17)$$

where $D^{(m)}$ is the binary diffusion coefficient of species m with respect to an abundant species. The species mass diffusion flux is then calculated from

$$J^{(m)} = -\rho D^{(m)} \nabla Y^{(m)} \quad (3.18)$$

It is possible to use tabulated data for diffusion coefficients and solve the species transport equations, however a more simplified formulation can be obtained by assuming equal Schmidt numbers for all species which results in equation 3.19. The effects of this approximation in laminar flame calculations of a methane/air mixture are presented in appendix B.

$$J^{(m)} = -\rho D \nabla Y^{(m)} \quad (3.19)$$

The species transport equations with this approximation, equation 3.20, are used in the present work. The diffusion flux term in energy equation is also modified with this assumption according to equation 3.21.

$$\frac{\partial(\rho Y^{(m)})}{\partial t} + \frac{\partial(\rho u_j Y^{(m)})}{\partial x_j} = \frac{\partial}{\partial x_j} \left(\rho D \frac{\partial Y^{(m)}}{\partial x_j} \right) + S^{(m)} \quad (3.20)$$

$$q_j = -\lambda \frac{\partial T}{\partial x_j} + \sum_{n=1}^N J_j^{(n)} h^{(n)} = -\lambda \frac{\partial T}{\partial x_j} - \sum_{n=1}^N \rho D \frac{\partial Y^{(n)}}{\partial x_j} h^{(n)} \quad (3.21)$$

3.2 Combustion Modeling

The set of flow equations presented in the previous section are closed and can be solved without any modeling assumptions using DNS methods. However, the grid resolution needed for such DNS numerical simulations is well above the capabilities of today's computers for practical

engineering flows. Other CFD methods such as RANS and LES turbulence models can be used for solving the flow of the mixture, however the effects of composition changes need to be in some way incorporated into these equations. One way to get this composition is to directly solve the species transport equations. This method is used in the present work.

Favre averaging and Favre filtering are well accepted methods of averaging/filtering varying density flows in LES and RANS turbulence models. This filtering results in the simplest formulation of filtered equations which best resemble the corresponding constant density formulations. The filtered conservation equations for multi-species systems are similar to their single species counterparts except for the extra diffusion term discussed earlier which is Favre filtered according to

$$\bar{q}_{j,extra} = -\overline{\sum_{n=1}^N \rho D \frac{\partial Y^{(m)}}{\partial x_j} h^{(m)}} = -\sum_{n=1}^N \bar{\rho} D \frac{\partial \widetilde{Y^{(m)}}}{\partial x_j} h^{(m)} \quad (3.22)$$

The Favre-filtered species transport equations are

$$\frac{\partial \bar{\rho} \widetilde{Y^{(m)}}}{\partial t} + \frac{\partial (\bar{\rho} \tilde{u}_j \widetilde{Y^{(m)}})}{\partial x_j} = \underbrace{\frac{\partial}{\partial x_j} \left(\rho D \frac{\partial Y^{(m)}}{\partial x_j} \right)}_I - \underbrace{\frac{\partial}{\partial x_j} [\bar{\rho} \widetilde{u_j Y^{(m)}} - \tilde{u}_j \widetilde{Y^{(m)}}]}_{II} + \underbrace{\bar{S}^{(m)}}_{III} \quad (3.23)$$

There are four extra terms, compared to single-species systems, which need modeling. These terms are the filtered extra diffusion term and three terms on the right hand side of the filtered species transport equations. The extra heat diffusion term and term I in equation 3.23 are easier to model and can be modeled as

$$\sum_{n=1}^N \bar{\rho} D \frac{\partial \widetilde{Y^{(m)}}}{\partial x_j} h^{(m)} = \sum_{n=1}^N \bar{\rho} D \frac{\partial \widetilde{Y^{(m)}}}{\partial x_j} \tilde{h}^{(m)} \quad (3.24)$$

$$\frac{\partial}{\partial x_j} \left(\rho D \frac{\partial Y^{(m)}}{\partial x_j} \right) = \frac{\partial}{\partial x_j} \left(\bar{\rho} D \frac{\partial \widetilde{Y^{(m)}}}{\partial x_j} \right) \quad (3.25)$$

Term II is the so-called turbulent transport flux term and is responsible for the enhancement of mixing of the species by turbulence. This is the turbulent diffusive flux of reacting scalars and can be modeled the same way the non-reactive scalars are modeled through gradient-diffusion models based on Boussinesq's hypothesis, equation 3.26.

$$(\widetilde{u_j Y^{(m)}} - \tilde{u}_j \tilde{Y}^{(m)}) = -D_t \frac{\partial \tilde{Y}^{(m)}}{\partial x_j} \quad (3.26)$$

The extra diffusion term involves the species diffusion flux $J^{(m)}$, equation 3.21, which can now be modeled using laminar and turbulent diffusion fluxes, equations 3.25 and 3.26. This choice of modeling the filtered extra diffusion term is consistent with the rest of the equations and is used here:

$$\bar{q}_{j,extra} = \bar{\rho}(D + D_t) \frac{\partial \tilde{Y}^{(m)}}{\partial x_j} \tilde{h}^{(m)} \quad (3.27)$$

The chemical source term, term III, is the most challenging term to model. The chemical source term is usually an exponential function of temperature and species mass fractions, therefore filtered sources involve correlations of temperature and mass fractions. There are several techniques to model this term. This term can be closed, no modeling needed, if the joint Probability Density Function (PDF) of temperature and species mass fractions is known. This is the so-called PDF transport technique in which the joint PDF of several flow properties is solved and is used to directly compute and close some of the terms, e.g. the chemical source term. There are a number of approaches for which PDF function to consider such as composition joint PDF, velocity-composition joint PDF, etc. The PDF transport models are computationally expensive, however they can be solved using Monte-Carlo methods for simpler cases. Details of this method can be found in Pope (1990, 1985).

The flamelet structure based combustion modeling is another approach to overcome the problem of the source term modeling. The flame in the corrugated flamelets and thin reaction zones regimes is quasi laminar and the flame structure follows that of a laminar flame. Therefore the scales of the flame and turbulence are separated and the flame is a thin layer that does not interact with the flow. Under such conditions it is possible to treat the flame as a freely propagating surface in the flow which gives feedback to the flow through density changes. The flow condition at this surface, flame front, works as the boundary condition to the laminar flame. These laminar flame structures under different conditions can be calculated separately using one-dimensional laminar flame calculations. The level-set G-equation technique belongs to this category of models and is presented in detail in Peters (2000).

The third option is to use reaction based techniques in which the source term is directly modeled using filtered flow properties (temperature and species mass fractions). The simplest approach is to directly

use the filtered properties in the Arrhenius reaction rate expression. This is very easy to apply but gives large errors. It is also possible to use linearized reaction rate expressions using Taylor series, however such series need many terms to converge and are impractical.

3.3 Finite Rate Chemistry

Chemistry time scales are often much smaller than turbulence time scales. This implies that the thin reaction regions can be treated as discontinuity surfaces. Sometimes the chemistry is assumed to be infinitely fast and no details of the reaction zones are taken into account in combustion modeling. These models are called infinitely fast chemistry models versus finite rate chemistry models in which the structure of the flame is in one way or another considered in combustion modeling. Techniques such as the level set G-equation model are finite rate chemistry models in this categorization since the structure of the flame is taken into account in laminar flamelet calculations. Nevertheless, finite rate chemistry models in the context of present work refer to combustion models in which the flame front structure is directly resolved in the simulation using rate based modeling of the chemical source terms.

In such finite rate chemistry models a difficulty is encountered as the typical grid size, both in RANS and LES, is larger than the flame thickness. Therefore, the flame can not be resolved in the computational domain. The flame needs to be at least as thick as one grid cell; however, the source term is very sensitive to even smallest temperature changes due to its exponential nature. This sensitivity results in variations in heat release and is a source for onset of non-linear numerical instabilities. These instabilities can cause large spurious oscillations when the flame is resolved in only one computational cell and might even result in divergence of numerical schemes. The artificially thickened flame technique (Butler & O'Rourke (1997); Colin *et al.* (2000)) is one solution to this problem. The flame in this technique is thickened over a number of computational cells while its laminar flame speed is preserved. The source term is then distributed in several cells and the heat release does not cause non-linear instabilities.

The finite rate chemistry method, coupled with thickened flame concept, has several advantages over other techniques.

- From a numerical point of view, the chemical reactions are described as in DNS on an LES grid. If the flame is thickened enough the actual flame is replaced by a thicker flame without filtering. This indicates that no subgrid modeling is needed for

the source term and the chemical source term is given by the reaction rates from the reaction mechanism evaluated by filtered variables.

- The reaction rates are given by Arrhenius expressions, therefore various phenomena, such as ignition, quenching, flame stabilization, flame-wall interactions, etc., are directly taken into account without extra modeling considerations.
- This approach can be used together with any reaction mechanism at any level of complexity.
- It is very easy to implement in CFD solvers. Moreover, the problem remains a convection-diffusion problem, there are no extra numerical methods needed.

Nonetheless, the increased flame thickness modifies the Damköhler number and consequently the interactions of turbulence with the flame are affected. The increased Damköhler number indicates that the flame response to turbulence is reduced and some of the flame surface is lost. Moreover, the structure of the flame might be affected by the turbulent eddies which now can penetrate into the thickened reaction zone. These effects are more important at high turbulence levels and complex chemistry.

Two different finite rate chemistry models are used in this thesis. For LSB studies an upwind thickened flame concept is applied which is similar to the artificially thickened flame technique. In this model the flame is not thickened explicitly and the thickening level is not decided in advance; instead, the numerical stability constraints dynamically thicken the flame in such a way that the numerical scheme is stable. The Total Variation Diminishing (Laney (1998); Eriksson (1995)) technique is used as the non-linear stability control mechanism. The reaction rates are given by the Meredith reaction mechanism and are corrected for turbulence and flame thickening effects. This technique is explained in detail in paper IV and is compared to the artificially thickened flame technique.

The PDE studies do not need to address any turbulence-chemistry interactions, therefore the reaction rates given by the reaction mechanism are not corrected. Instead, the reactions rate coefficients in the Arrhenius expression of the single step reaction mechanism are tuned to assure the onset of detonation under certain circumstances.

3.4 Governing Equations

The Unsteady Favre-filtered Reynolds-Averaged Navier-Stokes (URANS) equations for a multi-species system in conservative form with a realizable k-epsilon turbulence model can be written in compact form as

$$\frac{\partial Q}{\partial t} + \frac{\partial \mathcal{F}_j}{\partial x_j} = \mathcal{H} \quad (3.28)$$

The state vector Q in conservative form is given by equation 3.29 where $\bar{\rho}$ is the ensemble averaged density and, \tilde{u}_i , $\tilde{e}_0 = e + \frac{1}{2}\tilde{u}_m\tilde{u}_m + \tilde{k}$, $\tilde{Y}^{(m)}$, \tilde{k} and $\tilde{\varepsilon}$ are Favre-filtered velocity, total internal energy, mass fraction of species m , turbulent kinetic energy and turbulent dissipation rate respectively.

$$Q = \begin{bmatrix} \bar{\rho} \\ \bar{\rho}\tilde{u}_i \\ \bar{\rho}\tilde{e}_0 \\ \bar{\rho}\tilde{Y}^{(m)} \\ \bar{\rho}\tilde{k} \\ \bar{\rho}\tilde{\varepsilon} \end{bmatrix} \quad (3.29)$$

Equation 3.30 gives the flux vector \mathcal{F}_j where \bar{p} is the ensemble averaged pressure, τ_{ij} is the viscous stress tensor, $\tilde{h}_0 = \tilde{e}_0 + \frac{\bar{p}}{\bar{\rho}}$ is the total enthalpy, C_p is the specific heat at constant pressure, μ and μ_t are laminar and turbulent viscosity, Pr and Pr_t are laminar and turbulent Prandtl number, \tilde{T} is the Favre-filtered temperature, Sc and Sc_t are laminar and turbulent Schmidt numbers, $\tilde{h}^{(m)}$ is the Favre-filtered enthalpy of species m and σ_k and σ_ε are constants in the k-epsilon turbulence model.

$$\mathcal{F}_j = \begin{bmatrix} \bar{\rho}\tilde{u}_j \\ \bar{\rho}\tilde{u}_i\tilde{u}_j - C_p \left(\left(\frac{\mu}{Pr} + \frac{\mu_t}{Pr_t} \right) \frac{\partial \tilde{T}}{\partial x_j} \right) - \tilde{u}_i\tau_{ij} - \sum_{n=1}^N \left(\frac{\mu}{Sc} + \frac{\mu_t}{Sc_t} \right) \tilde{h}^{(n)} \frac{\partial \tilde{Y}^{(n)}}{\partial x_j} \\ \bar{\rho}\tilde{u}_j\tilde{e}_0 - \left(\frac{\mu}{Sc} + \frac{\mu_t}{Sc_t} \right) \frac{\partial \tilde{e}_0}{\partial x_j} \\ \bar{\rho}\tilde{k}\tilde{u}_j - \left(\mu + \frac{\mu_t}{\sigma_k} \right) \frac{\partial \tilde{k}}{\partial x_j} \\ \bar{\rho}\tilde{\varepsilon}\tilde{u}_j - \left(\mu + \frac{\mu_t}{\sigma_\varepsilon} \right) \frac{\partial \tilde{\varepsilon}}{\partial x_j} \end{bmatrix} \quad (3.30)$$

The viscous stress tensor is approximated with a Boussinesq's assumption as

$$\tau_{ij} = (\mu + \mu_t) \left(2\tilde{S}_{ij} - \frac{2}{3} \frac{\partial \tilde{u}_k}{\partial x_k} \delta_{ij} \right) - \frac{2}{3} \bar{\rho} \tilde{k} \delta_{ij} \quad (3.31)$$

C_μ	$C_{\varepsilon 1}$	$C_{\varepsilon 2}$	σ_k	σ_ε	Pr_t	S_{C_t}
0.09	1.44	1.92	1.0	1.3	0.9	0.9

Table 3.1: Constants in the k-epsilon turbulence model

where \tilde{S}_{ij} is the Favre-filtered strain rate tensor defined as

$$\tilde{S}_{ij} = \frac{1}{2} \left(\frac{\partial \tilde{u}_i}{\partial x_j} + \frac{\partial \tilde{u}_j}{\partial x_i} \right) \quad (3.32)$$

The source term \mathcal{H} is given by equation 3.33 where P_k is the turbulent production term, equation 3.35, and $C_{\varepsilon 1}$, $C_{\varepsilon 2}$ and C_μ are constants in the k-epsilon turbulence model. The various constants in the turbulence model are listed in table 3.4.

$$\mathcal{H} = \begin{bmatrix} 0 \\ 0 \\ 0 \\ \tilde{S}^{(m)} \\ P_k - \bar{\rho} \tilde{\varepsilon} \\ (C_{\varepsilon 1} P_k - C_{\varepsilon 2} \bar{\rho} \tilde{\varepsilon}) \frac{\tilde{\varepsilon}}{k} \end{bmatrix} \quad (3.33)$$

$$P_k = \left(\mu_t \left(2\tilde{S}_{ij} - \frac{2}{3} \frac{\partial \tilde{u}_k}{\partial x_k} \delta_{ij} \right) - \frac{2}{3} \bar{\rho} \tilde{k} \delta_{ij} \right) \frac{\partial \tilde{u}_i}{\partial x_j} \quad (3.34)$$

The realizability constraints is given by

$$\mu_t = \min \left(C_\mu \bar{\rho} \frac{\tilde{k}^2}{\tilde{\varepsilon}}, \frac{0.4 \bar{\rho} \tilde{k}}{\sqrt{\tilde{S}_{ij} \tilde{S}_{ij}}} \right) \quad (3.35)$$

The set of equations presented above represent realizable URANS equations and were directly used in PDE studies. However, the same set of equations can be used to perform LES studies of LSB. This set of equations also represent spatially Favre-filtered governing equations and the URANS model can be transformed to a hybrid LES/URANS model if a proper upper limit is imposed on the turbulent length scale. The details of this technique are discussed in Olausson (2011) and are presented in appendix C.

Chapter 4

Summary of Papers

THIS CHAPTER gives a short summary of the work done and the results reported in the five papers on which this thesis is based.

4.1 Paper I

4.1.1 Motivation and Background

A proper inlet boundary condition was needed for numerical study of the low swirl burner, however no well-defined and accepted boundary condition was available. A few experimental pieces of information were available which at the time were used by other groups for specifying the inlet velocity profile. The velocity profiles at several distances above the nozzle exit were measured and the one $2mm$ above was superimposed by synthesized turbulence and used as the inlet boundary condition by other researchers. This choice of boundary condition had led to elimination of the whole nozzle from computational domain, hence giving a very simple computational grid with simple cartesian grid cells. The mass flow split between the perforated-plate and the swirler-vanes was measured in a separate experimental study with the nozzle cap removed. Although the configuration of the burner was altered for this measurement, yet the results were considered by some groups to represent the mass flow split in the original configuration. The measured mass flow split figure was then used in some studies to extend the computational grid back to partly include the nozzle and the swirler-vanes but not the perforated-plate. The study presented in this paper suggested a third option in specifying the inlet boundary condition based on the computational domain shown in figure 4.1(a).

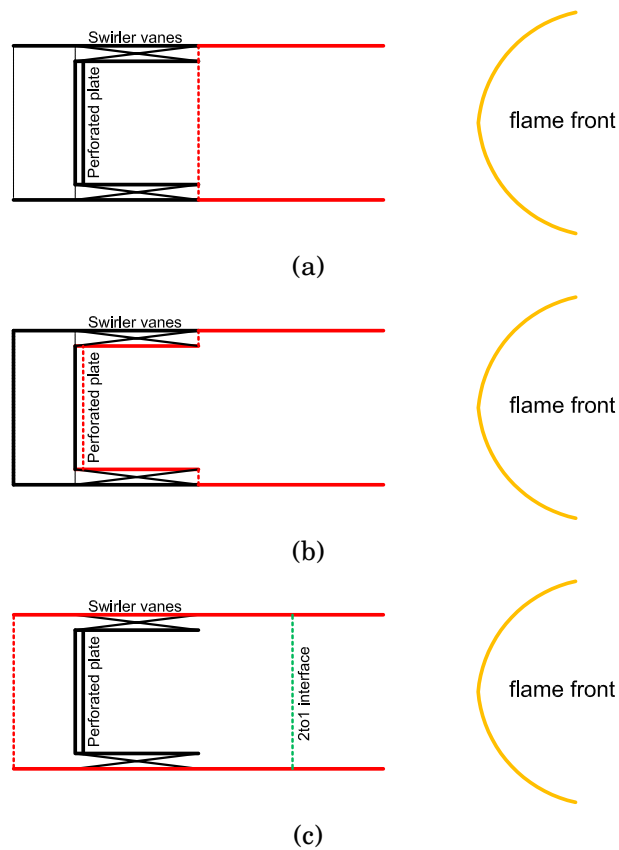


Figure 4.1: Schematics of the computational domain used to simulate the low swirl burner. Solid and dotted lines represent walls and inflow boundaries respectively. The red color shows the borders of the computational domain in each case. These figures illustrate only the boundaries inside the nozzle. Premixed methane/air mixture enters from left.

4.1.2 Work and Results

The flow field in the low swirl burner is of low velocities and it was not economical to solve it with a standard compressible flow solver. Therefore, the first step in simulating the low swirl burner flow field was to find the proper preconditioning level for the range of velocities in the flow. This was found by gradually decreasing the effective speed of sound to reach the state at which the results would be affected by further decreasing the speed of the acoustic waves. The chosen preconditioning value slows down the acoustic waves to values for which the whole domain is within the practical incompressible limit ($M_{eff} < 0.3$).

The next step was to find the proper inlet boundary condition. The total mass flow rate through the inlet and the measured mean velocity profiles $10mm$ downstream of the nozzle exit where available. Based on these information several candidate profiles were imposed as the inlet boundary condition in the computational domain shown in figure 4.1(a) and the one giving the best comparison of mean flow variables with the measured data $10mm$ above the nozzle was chosen as the inlet boundary velocity profile.

The previous steps were done using a coarse computational grid in single processor computations. The grid spacing was halved in all three directions into a fine computational grid which was then used for subsequent studies. The inlet profile was then used in the fine grid simulations to investigate the grid resolution effects on the problem. At this stage the solver was parallelized using MPI libraries to reduce the computational time.

A single reaction mechanism, equation 4.1, was considered where s is the stoichiometric ratio by weight.



The results showed that the flow field compares well with the experimental data indicating that the choice of the inlet profile is valid for both coarse and fine grid simulations. However, the temperature field showed some discrepancy from available experimental data in both coarse and fine grid simulations. The flame position in the coarse grid case was adjusted to the measured position by tuning the combustion model but it did not predict the dynamic flame structures. The fine grid case exhibited a hole in the core region, however at the time of submitting this paper the fine grid simulations had not yet been completed.

4.1.3 Comments

The combustion modeling needed to be simple at this stage as the focus was on the boundary condition problem and not the combustion modeling. The combustion model used in the simulations was a flame capturing combustion model which assumes that the flame propagation is governed by diffusion of species. Figure 4.2 shows a flame stabilized in a flow moving with velocity S_F to the right. It is assumed that reactions start at a threshold fuel mass fraction $Y_L^{Fu.}$, therefore the temperature and fuel mass fraction upstream of the flame front are only affected by convection-diffusion and not by reactions (heat release). Equation 4.2 gives the governing equation for flame propagation. Solving these equations assuming continuity of $Y^{Fu.}$ and $dY^{Fu.}/dx$ at $Y^{Fu.} = Y_L^{Fu.}$ gives the reaction rates, equation 4.3, which is similar to results given by laminar flame propagation theory of Mallard and Le Chatelier.

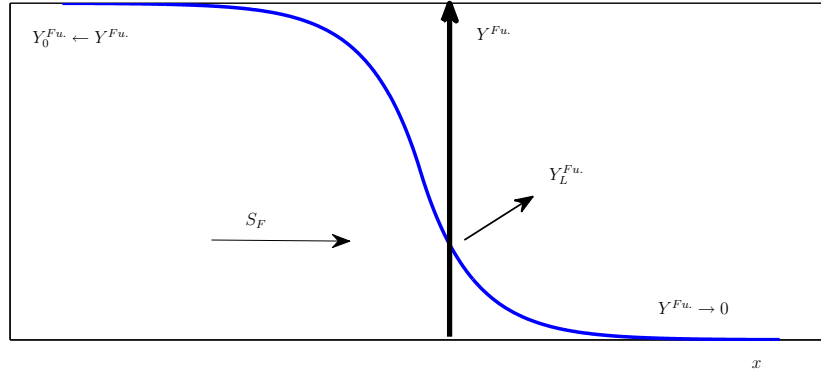


Figure 4.2: Flame stabilized at free stream velocity S_F

$$\begin{cases} S_F \frac{dY^{Fu.}}{dx} = \nu \frac{d^2 Y^{Fu.}}{dx^2} & \text{for } Y^{Fu.} > Y_L^{Fu.} \\ S_F \frac{dY}{dx} = \nu \frac{d^2 Y^{Fu.}}{dx^2} - A_k Y^{Fu.} & \text{for } Y \leq Y_L^{Fu.} \end{cases} \quad (4.2)$$

$$A_k = \left[\left(\frac{Y_0^{Fu.}}{Y_L^{Fu.}} - \frac{1}{2} \right)^2 - \frac{1}{4} \right] \frac{S_F^2}{\nu} = C \frac{S_F^2}{\nu} \quad (4.3)$$

4.2 Paper II

4.2.1 Motivation and Background

The fine grid simulations which was started with paper I needed to be completed to evaluate the potential of the combustion model in pre-

dicting the flame position and dynamics. Furthermore, only the mean velocity field was compared with experimental data in paper I whereas the fluctuations of the velocity field could have a significant role in flame dynamics. Therefore, further studies were performed which resulted in paper II.

4.2.2 Work and Results

The final fine grid simulations revealed that the hole in the core region of the flame was inevitable, nonetheless its depth was eventually reduced compared to the results presented in paper I. In addition to existence of this hole, the flame in the core region did not exhibit the dynamic behavior observed in the experiments. One possible cause of this discrepancy was the lack of turbulent flow structures in the core region which result from the jets emanating from the holes in the perforated-plate. It was observed that the velocity fluctuations measured at the flame front region were significantly larger than the laminar flame speed of the mixture. This suggests that these structures can significantly wrinkle the flame in the core region and cause the flame dynamics observed in experimental results. Therefore, as a further step in simulating the flow-flame field, the effects of these holes were added at the inlet by extending the computational domain back to the location of the perforated plate, figure 4.1(b). Preliminary results, available at the time of paper submission, showed that adding these jets lead to the appearance of large scale turbulence in the core region and the flame became very dynamic in that area. The velocity fluctuations were better predicted compared to results from paper I, however the mean axial velocity showed deviation from experimental data specially in the core region where a high axial velocity appeared in the center.

4.2.3 Comments

One important factor which determines the swirl number is the radial velocity distribution across the nozzle. Although the inlet boundary condition in paper I was adjusted to give correct swirl number at the inlet, adding the holes changed the swirl number. The uniform flow assumed at the inlet in paper I was replaced here by the non-uniform flow evolved from interactions of the jets. This discrepancy needed to be readjusted since the simulations performed had revealed high dependence of the flow field and flame structures on the swirl number. The problem of finding the proper boundary condition was not yet solved at

this stage, therefore combustion modeling was not yet in focus and the same simple combustion model as paper I was used.

4.3 Paper III

4.3.1 Motivation and Background

The primary studies on pulse detonation engine, presented in the unpublished results chapter, revealed that direct substitution of the combustor in a conventional aircraft engine frame with a set of pulse detonation tubes causes severe problems at compressor side when multiple tubes with a controlled firing sequence is applied. A few suggestions were made to overcome this problem of which the statorless configuration method for replacing the combustor with a set of pulse detonation tubes was studied in this paper.

4.3.2 Work and Results

Two alternative PDE configurations were compared in this paper. In the first configuration the combustor is directly replaced by a set of detonator tubes, figure 4.3. The second configuration was based on a statorless turbine in which the HPT stator row was eliminated and instead the detonation tubes were bent to directly discharge the flow at the proper angle into the turbine, figure 4.4. Both synchronized and non-synchronized firing sequences were considered. In the primary studies of PDE the valve was simulated as walls during the spark and detonation/blowdown phases and as specified mass flow during fill and purge phases. This boundary condition assumes that the mass flow through the engine is not affected by the flow condition in the combustor. In other words, the compressor side will immediately adapt itself to the combustor in such a way that during fill and purge phases a steady mass flow is injected into the tubes. The valve was simulated with the following boundary conditions in this paper.

- during the spark and detonation-blowdown phases it is defined as a solid wall.
- during the purge and fill phases it changes from open position to closed position instantaneously if the flow reverses through it and changes from closed position to open position when the pressure at the tube side drops below the pressure at the compressor side.

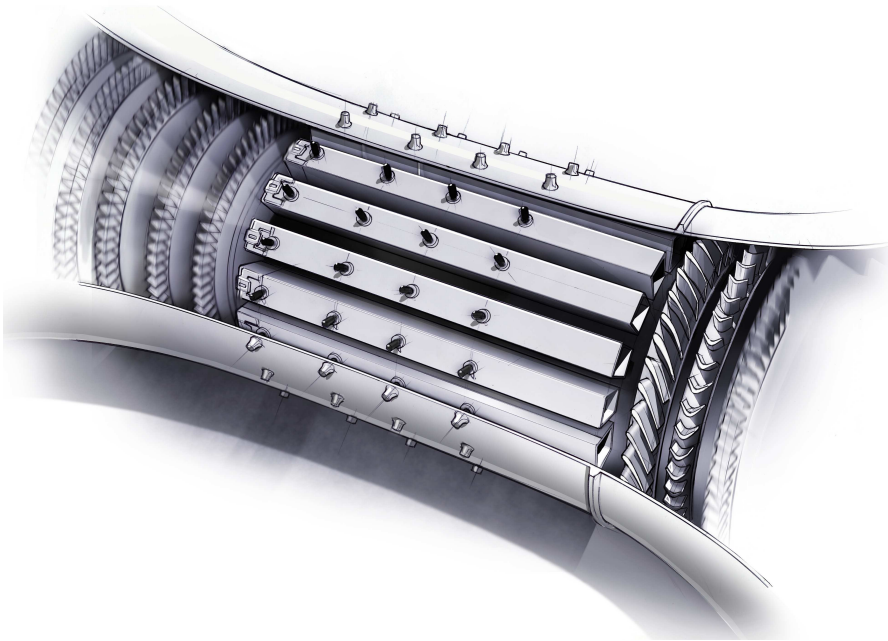


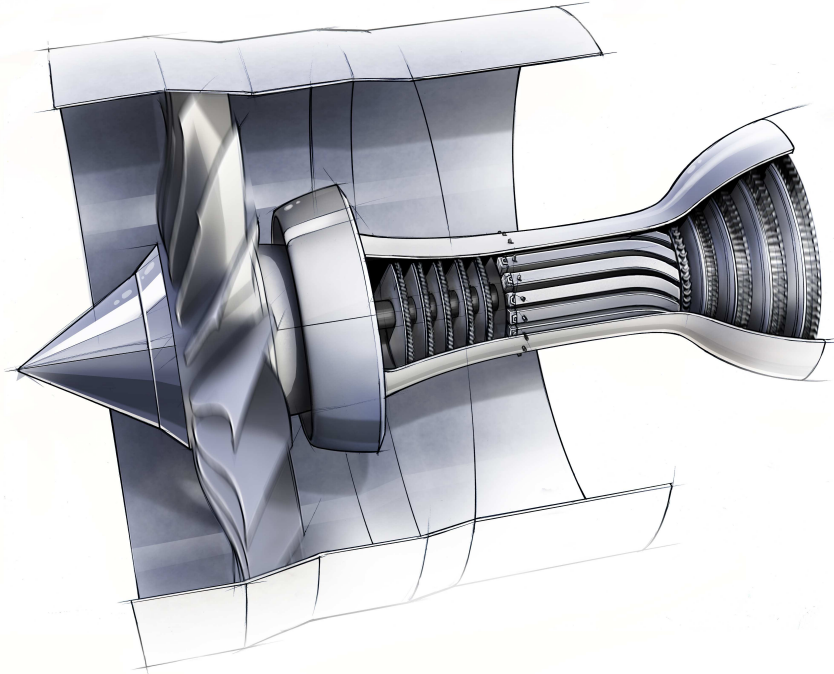
Figure 4.3: PDC integration in a PDE, direct substitution (Chalmers University ©).

The results show that the statorless turbine configuration offers a wider range of operating conditions while the problem of traveling waves in adjacent tubes in the first configuration is a serious problem which poses high limitations on working conditions of PDE, specially when a non-synchronized firing is applied.

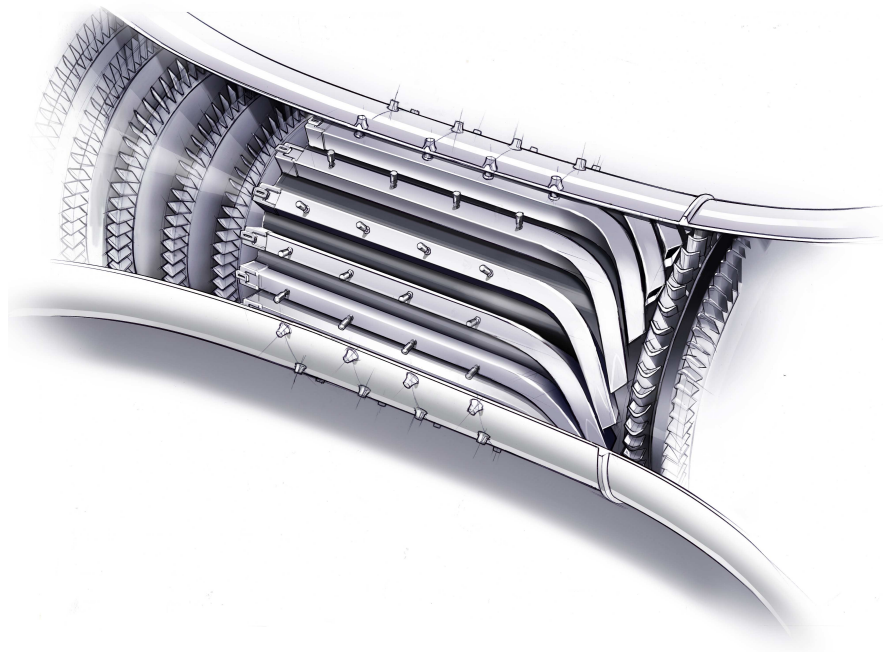
4.3.3 Comments

The gas properties in this work were slightly modified so that the conditions at Chapman-Jouguet plane were met at the burned side. The simple test case used for validation showed that the correct detonation velocity was also predicted. The deflagration to detonation distance was also predicted within a reasonable limit, though the combustion model was not specifically tuned for this purpose.

One problem with the idea of the statorless turbine is that the high velocity flow should pass through the bent tube which is at a steep angle. This results in large regions of recirculation in the bent section. The flow passing from the compressor to the tubes however is at much lower velocity. Therefore, it is easier to turn the flow right at the tube inlet. This can be achieved by PDE configuration illustrated in figure 4.5. This configuration was not analyzed due to lack of time.



(a)



(b)

Figure 4.4: PDC integration in a PDE, statorless turbine PDE configuration (Chalmers University ©).

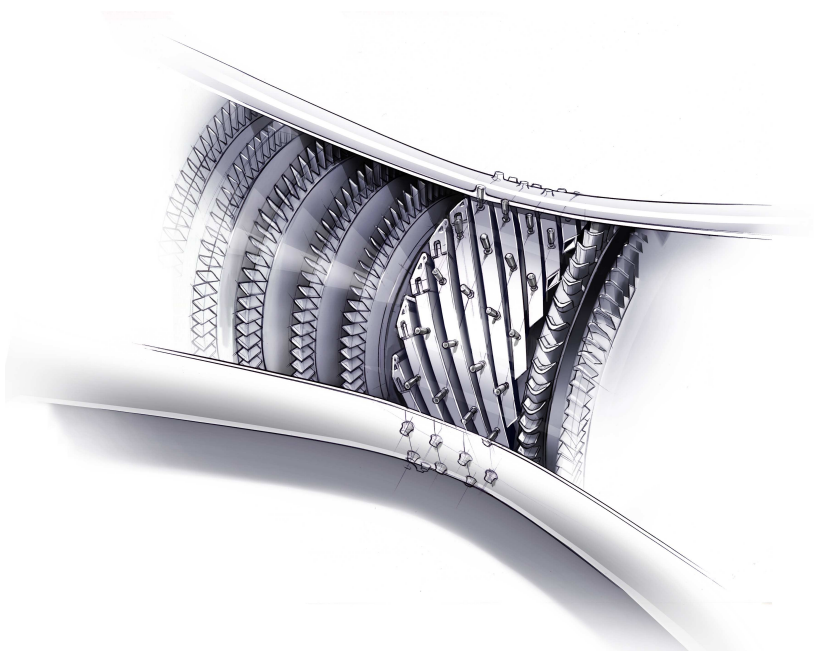


Figure 4.5: PDC integration in a PDE, tilted tube PDE configuration (Chalmers University ©).

4.4 Paper IV

4.4.1 Motivation and Background

Results obtained in papers I and II showed that a somewhat proper inlet boundary condition was found, therefore the focus shifted to combustion modeling in paper III.

4.4.2 Work and Results

A three step global reaction mechanism from literature was chosen and validated for laminar flame property predictions. The combustion model was also modified for better approximation of turbulent flame speed and effective viscosity. The combustion model was shown to work similar to a artificially thickened flame technique. However, applying an artificially thickened flame model resulted in blow out of the flame while the combustion model developed in this work gave a dynamic yet stable flame.

4.4.3 Comments

Addition of modeled holes helped the simulations in predicting the dynamic behavior of the flame front but the velocity profiles did not compare well with the experimental data. In particular, the high velocity in the center line resulted in a deep hole in the mean flame front.

4.5 Paper V

4.5.1 Motivation and Background

The results from previous papers indicated that there is still room for improvement in specifying the inlet boundary condition for LSB studies. In this paper the computational domain was extended back to include the perforated-plate/swirler-vanes component, figure 4.1(c), hence eliminating any assumption at the inlet.

4.5.2 Work and Results

A block structured grid was adapted to the now complicated geometry. The grid at the inlet side was twice as fine as the grid at the flame side separated by a 2-to-1 grid interface. Both reacting and non-reacting simulations were performed. The predicted mass flow split differed from the aforementioned measured values by 10%. The flame position and dynamics were well predicted and the flow field showed the well known characteristics of a low swirl flow field observed in several experiments.

The effects of mass flow split and effective vane angle were studied in several other simulations on computational grids previously used in papers I, II and IV. The results interestingly showed that it is possible to capture correct flame position along the center line, under certain inlet conditions, when the modeled holes are not included (figure 4.1(a)). However, the flow field does not represent a low swirl flow field and the flame dynamics are not well predicted. On the other hand, using modeled holes (figure 4.1(b)) with proper inlet conditions gives a dynamic flame but the flame position is not well predicted.

4.5.3 Comments

This study revealed that the flame dynamics are strongly connected to unsteady flow structures. These flow structures are mainly generated and evolved inside the nozzle. The flow interactions inside the nozzle

yield a complicated flow field with varying turbulence characteristics across the nozzle, hence a synthetic turbulence seems to be inadequate for resembling the turbulence at the nozzle exit. There are two ways to specify the inlet boundary turbulence in LSB numerical simulations. One is to extend the computational domain upstream to include the major parts which affect the flow unsteady structure. This method was used in this study and showed to be successful in flow-flame predictions. However, this option is numerically expensive. Nevertheless, it was shown in this paper that the flame front position and velocity fluctuations at the nozzle exit are not correlated. Thus, a time series of flow field at the nozzle exit can be extracted from this simulation and saved in a database which could be then imposed as the boundary condition in other numerical studies of this burner. Such boundary condition can be used to eliminate the whole nozzle from numerical studies, hence resulting in a simple cartesian grid which is favorable for computer codes. This simple geometry together with well defined and easy to use boundary conditions provided by this study make LSB a proper test case for evaluation of numerical methods specially LES combustion models.

Chapter 5

Unpublished Results

THIS SECTION gives some of the results from primary studies on PDE which motivated the study presented in paper III.

5.1 PDE Configuration

The combustion chamber in a PDE consists of a set of detonation tubes which fire periodically at a certain frequency. The tubes can either fire all at once, synchronized firing, or they can be out of phase following a controlled phase-shift firing sequence, non-synchronized firing. The integration of the PDC in the frame of a turbofan engine is not trivial. The simplest PDE consists of a set of detonation tubes directly exhausting in the air which provide the thrust necessary for the aircraft to fly. However, the PDC should be integrated in a conventional engine frame including turbomachinery to yield maximum benefits in efficiency. The first and most straightforward PDC integration method is to directly replace the combustion chamber in a turbofan engine with a set of tubes. Connected to each tube is a divergent part, diffuser, which will guide the flow toward the turbine stator guide-vanes. These tubes/diffusers are circumferentially distributed and connected to a plenum to which the stator guide-vanes are connected at the other side. This PDE configuration is sketched in figure 5.1 in which the diffuser angle is chosen to be zero. Each tube is directly followed by a guide-vane in this configuration, however the number of tubes and guide-vanes do not need to be necessarily equal. A 2-D cross section of this configuration is used in this numerical study, figure 5.2.

There is a pressure valve at the inlet of each tube, figure 5.1, which will open to let the flow into the tube when necessary and will close when the detonation process is started. This valve is not directly simulated in this work.

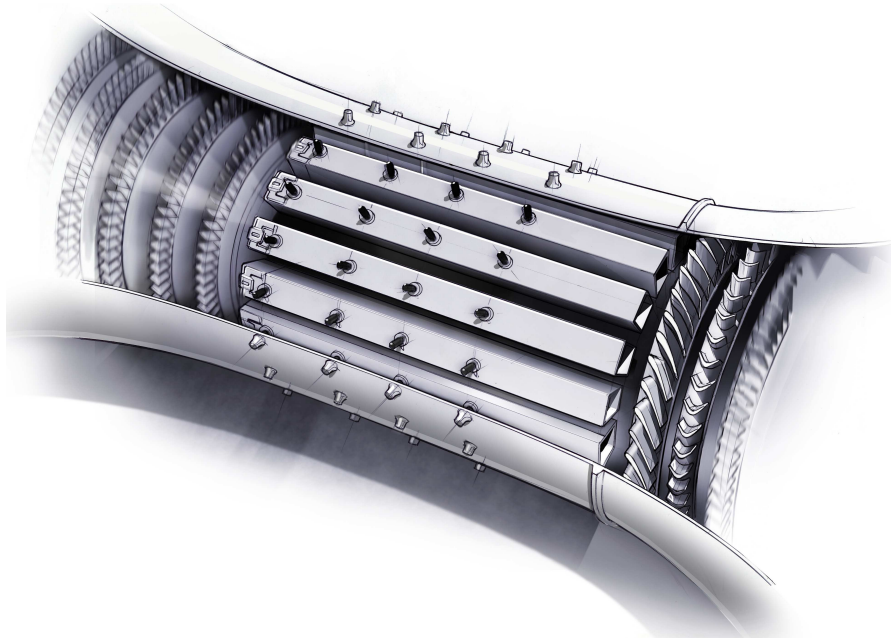


Figure 5.1: A conceptual PDE configuration in which the tubes directly replace the combustion chamber (Chalmers University ©).

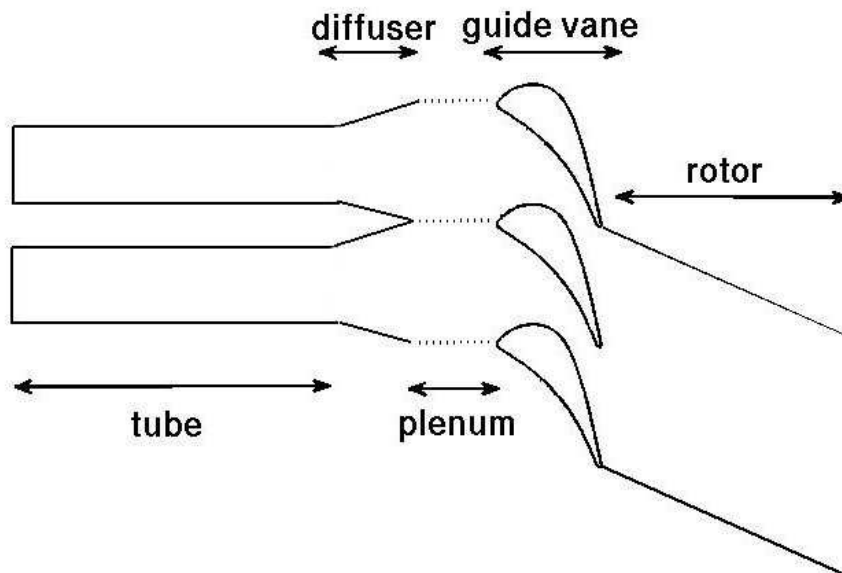


Figure 5.2: 2-D cross section of the PDE.

5.2 Pulse Detonation Cycle

The detonation cycle simulated in this work consists of four phases which are illustrated in Figure 5.3.

- In the *Purge* phase the input valve is opened and pure air flows into the tubes to sweep the combustion products away and to cool the tubes and the turbine blades.
- In the *Fill* phase the input valve is opened allowing the fuel/air mixture to flow into the tubes.
- In the *Spark* phase the valve is closed and a local spark near the valve initiates the combustion of the mixture which will eventually lead to detonation.
- In the *Detonation/Blowdown* phase the detonation wave evolves and the flow is developed until the next cycle starts to repeat the purge phase.

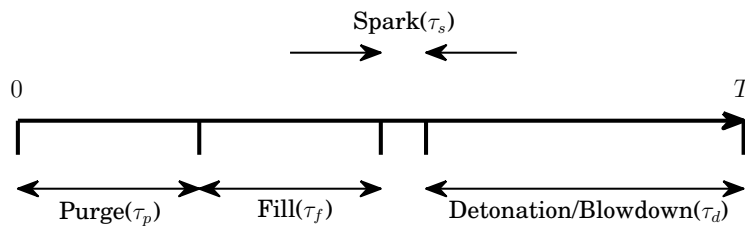


Figure 5.3: PDE working cycle.

5.3 Test Case

The test case simulated in this study is an engine at take off. The thermodynamic design parameters of the engine are chosen to represent a year 2010 entry of service engine. The fuel is Jet-A, the oxidizer is air and the mixture is stoichiometric. There are a number of considerations that should be addressed when setting up a conceptual PDE configuration:

- To establish the detonation in a tube, a minimum length of the tube must be filled with fuel/air mixture which should exceed the length needed for deflagration to detonation transition. Moreover, the width of the tube has to be selected carefully; the tube geometry should be chosen in such a way that a sufficient length of the tubes is filled with fuel/air mixture in the whole aircraft/engine mission.

- The idea of having a controlled phase-shift sequence of ignition in the tubes is to minimize the unsteadiness of the flow at the rotor inlet. To allow having several phase-shift options, the number of tubes should be carefully chosen so that one could find an integer number of tubes across which the flow is periodic in circumferential direction. Establishing the periodicity reduces the computational cost.
- Auto-ignition of the fuel/air mixture is a problem in high working pressure and temperature of the mixture at the inlet of the tubes. For the hot day take-off point studied here, the auto-ignition time for Jet-A/air mixture is in the order of $2.5 - 4ms$ for a premixed mixture at a lean equivalence ratio ($\phi = 0.7$). The auto-ignition time for the stoichiometric mixture is lower which suggests that the fuel/air mixture should be detonated before this time limit. In a real engine the fuel/air mixture is not premixed and the fuel is sprayed into the air, therefore the filling time can be increased if fuel/air contact time is reduced by proper fuel injection timing. The multi-point injection system shown in figure 5.1 is one example of providing proper fuel injection timing in which the tube is first filled with pure air then the fuel is injected at several points. Therefore, the fuel and air will not be in contact during the fill period, hence the risk of auto-ignition is reduced. Nevertheless, the filling time in this study was chosen not to substantially exceed these auto-ignition limitations. This short filling time also implies that the velocity of the mixture entering the tubes from compressor side should be high enough to fill a sufficient length of the tube.
- The fuel/air mixture is stoichiometric resulting in very high post-combustion temperatures. The purge air is used to cool the tubes and the turbine. The amount of purge air must be sufficient to reduce the average turbine entry temperature to values in the range of state of the art of turbine technology. In this work the purge air reduces the effective equivalence ratio to 0.4 which is a suitable value for a conventional engine design. The purge air also washes away the combustion products and provides a cold buffer layer between hot products and fresh reactants.

Based on the above limitations a conceptual engine is configured according to Table 5.1. The stator guide-vane design is chosen from a well known test case for transonic stators available in the public domain (Sieverding (1982)). The working conditions and the working cycle for the test case are given in table 5.2 and figure 5.4. Fuel injection is not

Number of tubes	36	Tip radius at HPC outlet	0.3798
Tube diameter	0.04	Hub radius at HPC outlet	0.3212
Tube length	0.60	Tip radius at HPT inlet	0.3670
Diffuser length	0.1	Hub radius at HPT inlet	0.3350
Diffuser angle	5°	Tip radius at HPT rotor inlet	0.3670
Plenum length	0.1	Hub radius at HPT rotor inlet	0.3350

Table 5.1: Test case engine dimensions, all lengths are given in meters.

considered and the fuel/air mixture entering the tubes is assumed to be fully premixed. The inlet temperature given here corresponds to both pure air and the fuel/air mixture.

Purge time, $\tau_p(ms)$	4.0	Fuel/air equivalence ratio, ϕ	1.0
Fill time, $\tau_f(ms)$	4.0	Effective equivalence ratio, ϕ_{eff}	0.4
Spark time, $\tau_s(ms)$	0.05	Inlet pressure, $P_{in}(bar)$	32
Det./B.D. time, $\tau_d(ms)$	8.0	Inlet temperature, $T_{in}(K)$	870
Period, $T(ms)$	16.0	Fuel Consumption Rate (kg/s)	1.2
Frequency, $f(Hz)$	62.5		

Table 5.2: PDE working cycle and working conditions.

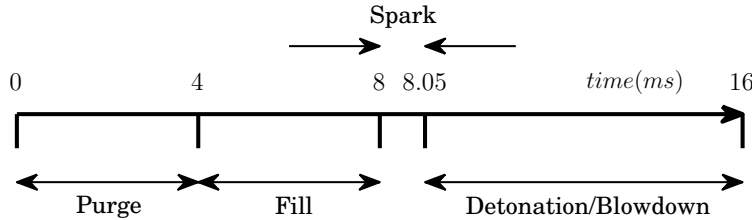


Figure 5.4: PDE cycle timing for synchronized firing test case.

5.4 Computational Domain

The computational domain and the grid adapted to the geometry are shown in Figure 5.5. The domain is a two-dimensional cross section of the PDE which starts at the tube inlet and includes the tube, the diffuser and one guide-vane. It then extends for some distance in axial direction. The grid does not include any turbine rotor row. In circumferential direction the grid should include a number of tubes which give

periodicity in that direction. In case of synchronized firing one tube represents such periodicity. The grid is block structured. It is refined in the boundary layers around the stator guide-vane walls, figure 5.5, and consists of around 11000 computational cells in total.

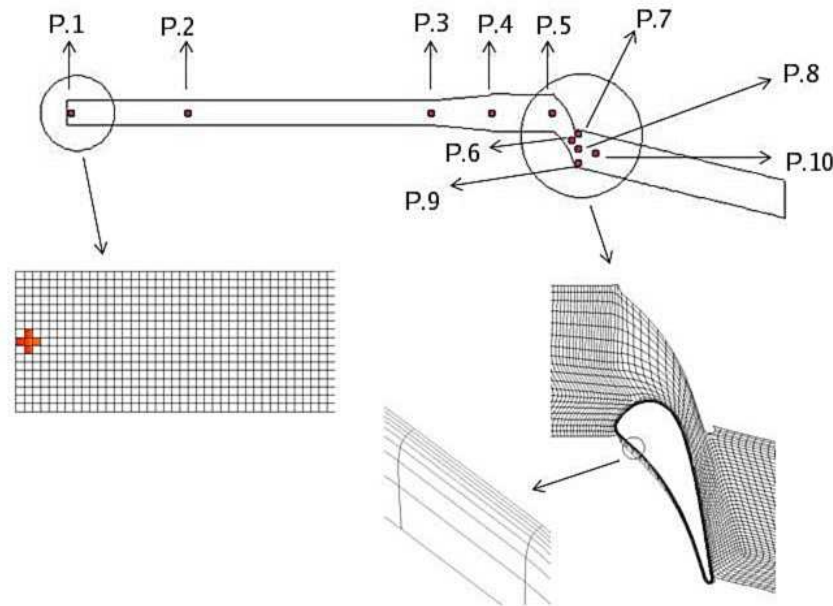


Figure 5.5: Computational domain (top), ignition cells (left), computational grid in guide-vane passage (right) and boundary layer grid (bottom). Several probes in the domain, top figure, record the time history of flow properties.

5.5 Numerical Method

Periodic boundary condition is applied in circumferential direction. The walls are set to no-slip walls and are treated with wall functions. The outlet is set to a specified pressure condition. However, to overcome convergence problems, specially in the beginning of the simulations, this pressure is allowed to vary to avoid suction into the exit plenum from outside of the domain. The simulations then run for several detonation cycles to ensure that a limit cycle, a condition at which flow properties do not change in successive cycles, is established. The tube inlet boundary condition depends on which phase is being simulated. In the fill and purge phases it is set to a specified mass flow boundary condition where a total mass flow at specified total enthalpy is prescribed. In this period the pressure, density and temperature at the inlet vary so that the prescribed mass flow at prescribed total enthalpy

enters the domain. In the spark and detonation/blowdown phases the inlet boundary condition is set to a no-slip wall. The spark which is responsible for combustion initiation is modeled as a local heat addition in five cells close to the tube inlet, figure 5.5. A number of probes are placed in the domain to record the variation of flow properties in time. These probes are shown in figure 5.5 and their geometrical locations are given in table 5.3.

P.1	Inlet	P.6	Guide-vane minimum area
P.2	20 cm from inlet	P.7	Guide-vane outlet (top)
P.3	End of the tube	P.8	Guide-vane outlet (middle)
P.4	End of the diffuser	P.9	Guide-vane outlet (bottom)
P.5	Guide-vane inlet	P.10	Rotor inlet

Table 5.3: The geometrical location of probes in the domain.

Unsteady RANS with standard $k - \varepsilon$ turbulence model together with wall functions are used for turbulence modeling. The numerical schemes used here are similar to other simulations presented in this thesis. The combustion model is based on a single reaction mechanism, equation 5.1, where s is the stoichiometric ratio by weight. Therefore, there are four species, Fuel, Oxygen, Products and Inerts, involved in the simulations of which the transport equation for the first three are solved. The fuel is aviation Jet-A fuel and the oxidizer is air in this work.



The reaction rate RR is given by a simple Arrhenius expression, equation 5.2, in which the pre-exponential factor A and activation energy E_a are adjusted so that onset of detonation is assured. The detonation is triggered by introducing a local heat source in the tube and with the aid of rapid heat release through exponential reaction rate the initial deflagration wave transforms to detonation. In order to avoid auto-ignition a threshold temperature, $T_L = 1200K$, is specified below which all reactions are neglected.

$$\begin{cases} RR = A\rho Y^{Fu} \cdot Y^{O_2} e^{-E_a/T} & \text{for } T > T_L \\ RR = 0 & \text{for } T < T_L \end{cases} \quad (5.2)$$

The species are assumed to be perfect gases, therefore the enthalpy and internal energy are functions of temperature only as indicated in equations 5.3 in which H_f is the heat of formation of species.

$$h = H_f + C_p T \quad e = H_f + C_v T \quad C_p = C_v + R \quad (5.3)$$

The gas constant R and the specific heat at constant pressure C_p for individual species are assumed to be constant. To find these gas properties the enthalpy versus temperature for all the species are found from NASA polynomials in the expected range of temperature using the well known NASA CEA code (McBride & Gordon (1996)). The species gas properties are then computed from a linear curve fit onto this data.

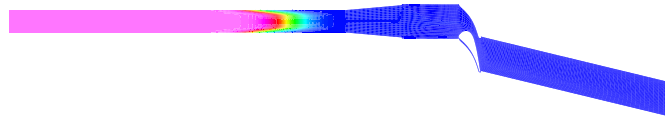
The detonation process is approximated by a constant volume combustion where the density and internal energy of the mixture do not change by combustion. The above procedure does not exactly results in these conditions at the burned side. Therefore, some of species gas properties, which are found by above curve fitting, are slightly modified so that the combustion takes place in a constant volume mode and the expected post-combustion pressure of the mixture is achieved. This is validated by comparison with results computed by CEA code.

5.6 Results

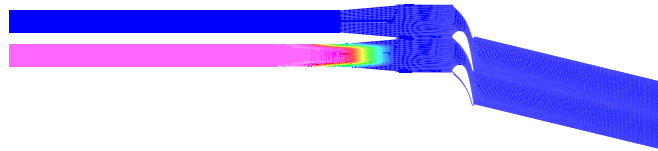
The initial state is defined as the tube filled with fuel/air mixture and the rest of the domain filled with cold products. The simulation starts with the spark phase and continues to reach a limit cycle condition as the effects of the initial conditions decay. This usually takes only a few cycles but here the computations are continued for ten cycles to ensure a well converged solution. The results presented in this section correspond to the last cycle. Figure 5.6(a) shows the contours of the fuel mass fraction at the end of the fill process indicating the extent to which the tube is filled with fuel/air mixture. This is a very important parameter for establishing a proper detonation wave. In this test case approximately $47cm$ of the tube is filled. Figure 5.7 gives a set of snapshots of temperature and pressure contours showing the propagation of the detonation wave in the domain. The first snapshot at the top corresponds to the end of the fill phase.

Figure 5.8 shows the time history of static pressure and Mach number at P.7, P.8 and P.9 locations. This figure illustrates the 2D behavior of the flow at the stator guide-vane outlet which indicates that the turbine rotor is exposed not only to time variations but also to spatial variations during the cycle. The flow is transonic for the major part of the cycle which confirms the choice of a stator guide-vane designed for transonic operation.

A second test case was studied to investigate the effects of a controlled phase-shift firing sequence on the working conditions of PDE. A



(a)



(b)

Figure 5.6: Contours of fuel mass fraction at the end of the fill process for synchronized (a) and non-synchronized (b) firing test cases.

set of two tubes with 180° out of phase working cycles are put together for this purpose. The cycle timing and the working conditions are exactly the same as the first test case. The cycle is depicted in figure 5.9.

Figure 5.6(b) shows the fuel mass fraction contours at the end of the fill phase which indicates that a larger portion of the tube length is filled with fuel/air mixture compared to the synchronized firing test case.

5.7 Fill Phase

Figure 5.10(a) shows a time series of static temperature and static pressure at P.1 for the synchronized firing test case. This probe is located at the inlet and shows the unsteady flow exerted on the compressor. The temperature is relatively constant at the inlet while the pressure undergoes slight variations. Figure 5.10(b) shows the corresponding results for the lower tube in the non-synchronized test case. The pressure variations for the non-synchronized firing test case are much higher in magnitude and can severely affect the working conditions at the compressor side. Figure 5.11(a) shows a series of snapshots of tem-

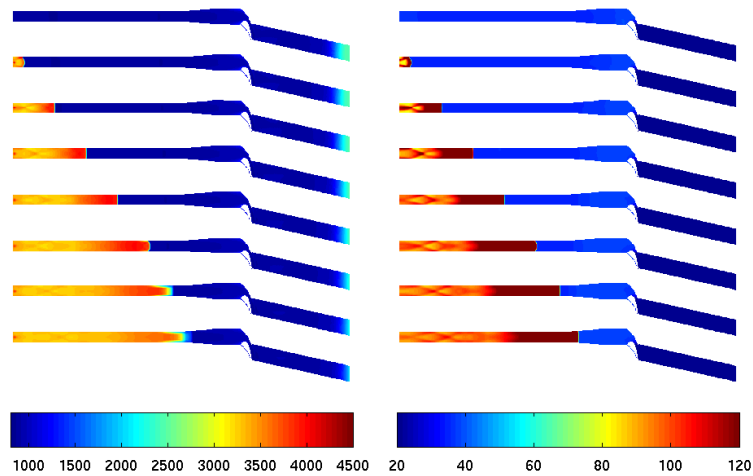


Figure 5.7: Propagation of detonation wave visualized by contours of static temperature (left) and static pressure (right). Snapshots are taken at $50\mu s$ intervals starting at the end of the fill period (snapshot at the top). Temperatures and pressures are in Kelvin and bars respectively.

perature and pressure contours for synchronized firing case. The detonation wave can not smoothly pass through the guide-vane passage and is repeatedly reflected back and forth by the closed valve and the stator guide-vane. Figure 5.11(b) shows the corresponding snapshots for the non-synchronized case which reveals that the detonation wave generated in one tube can enter the other tube, which is in purge phase, and travels all the way upstream to hit the compressor (figure 5.10(b)). The pressure magnitude is much higher in the non-synchronized case and can severely affect the compressor operating conditions. In a real engine the valve opens/closes according to the pressure difference across it. It lets the flow into the tube only when the pressure is lower in the tube side. However, these pressure variations can cause a higher pressure in the tube side and interrupt purge/fill process.

The idea of having a controlled firing sequence reduces the flow unsteadiness in the turbine inlet and it is worth to seek for a solution to avoid the unsteady flow exerted on the compressor side. One solution is to change the cycle timing by increasing the detonation/blowdown time so that the most severe pressure variations have passed before the purge phase starts in the adjacent tube. In the working cycle and engine configuration studied here the highest pressure peaks occur at around $9ms$ and $10ms$, therefore if the start of the purge phase is de-

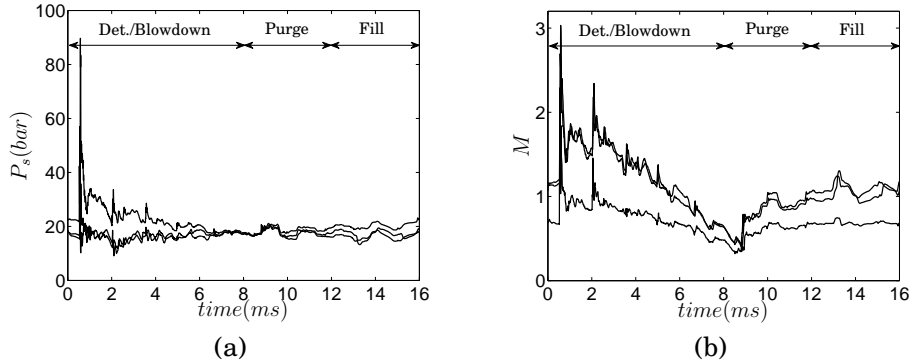


Figure 5.8: Time variation of static pressure (a) and Mach number (b) at probes P.7, P.8 and P.9 for synchronized firing test case, flow at P.7 shows different behavior compared with P.8 and P.9.

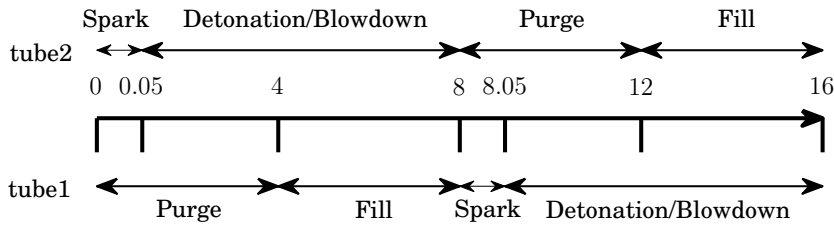


Figure 5.9: PDE cycle timing for two tubes firing 180° out of phase. Time periods are given in ms.

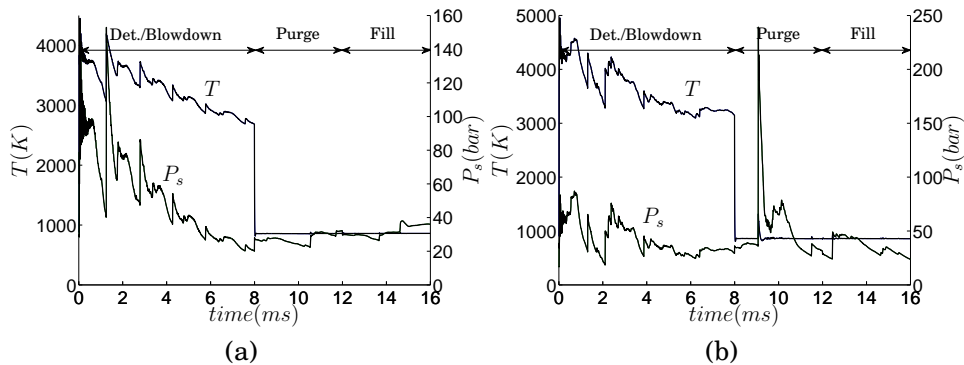
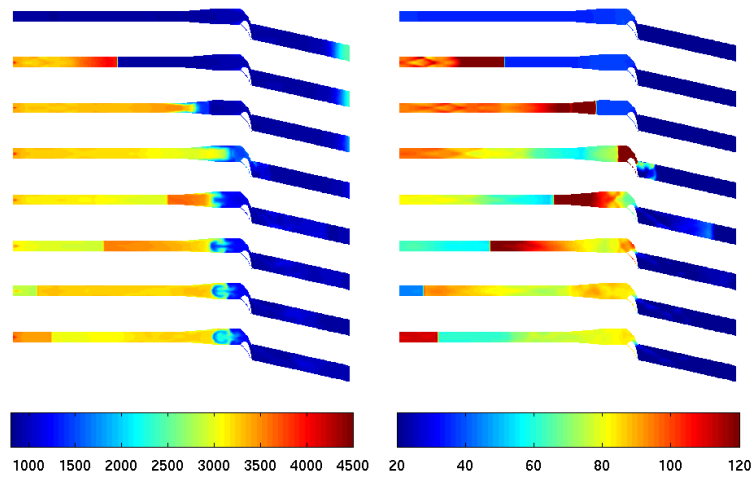
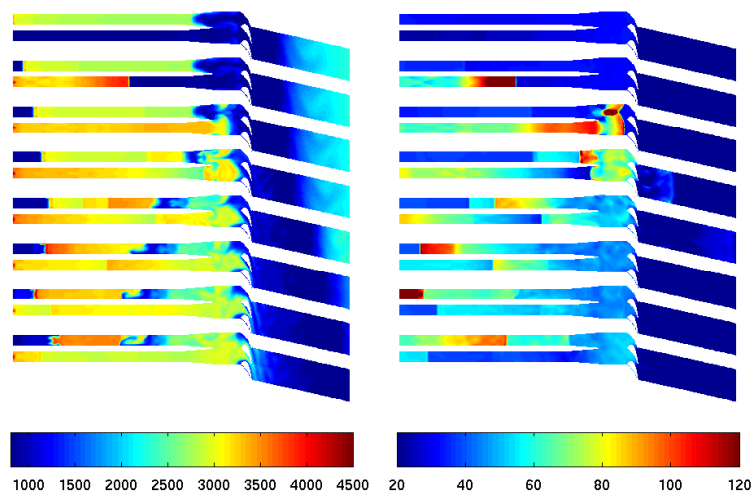


Figure 5.10: Time history of static pressure and static temperature at P.1 for synchronized firing case (a) and non-synchronized firing case (b).



(a)



(b)

Figure 5.11: Propagation of pressure waves in synchronized firing (a) and non-synchronized firing (b) test cases visualized by contours of static temperature (left) and static pressure (right). Snapshots are taken at $200\mu s$ intervals starting at the end of the fill period (snapshot at the top). Temperatures and pressures are in Kelvin and bars respectively.

laid past this time these pressure waves will not affect the compressor operation. This can be easily achieved by increasing the detona-

tion/blowdown phase time to $11ms$ while maintaining the duration of the fill and purge periods. However, this solution is not possible when a more complicated firing sequence is needed.

Another solution is to isolate the tubes from each other by means of solid walls. The plenum attached to the tubes can be split by parallel walls so that each tube is directly connected to its stator guide-vane via a channel. In this configuration non-synchronized firing can reduce the unsteadiness at the rotor inlet while the pressure waves can not enter the adjacent tubes and interfere with their fill/purge process.

A third solution is to further simplify the configuration by eliminating the stator row and instead directly bending the tubes toward the rotor row in a statorless turbine, figure 5.12. This PDE configuration has been studied in paper III.

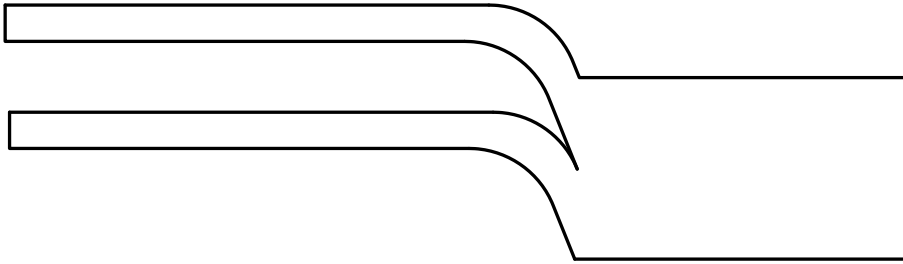


Figure 5.12: Bent tubes in a statorless turbine PDE configuration.

Chapter 6

Concluding Remarks

NUMERICAL METHODS are applied to study two different reacting flows: a low speed deflagration in a low swirl burner and a high speed detonation in a conceptual pulse detonation engine. In both cases, the combustion phenomenon is modeled by finite rate chemistry concept. However, the combustion modeling should address different phenomena in these two cases. In PDE studies performed in this work combustion modeling is not aimed at resolving the details of detonation phenomenon, instead it is tuned to ensure that detonation happens under specific initial conditions and it gives correct conditions at the burned side (Chapman-Jouguet conditions). In LSB studies on the other hand, flame propagation in the flow field which determines flame position, flame dynamics and flame stabilization mechanism is highly dependent on interactions of combustion and flow, turbulence-chemistry interactions, which are directly modeled through combustion modeling. The finite rate chemistry concept was able to meet the requirements for both flows studied here.

Previous numerical studies on LSB have all suffered from lack of proper inlet boundary conditions. The effects and importance of the inlet condition were investigated by considering several computational domains and their corresponding inlet conditions. The results show that the flame stabilization mechanism depends on the imposed inlet boundary condition. The flame is stabilized as the result of a delicate balance between deceleration of the flow in the core region, large scale motion of flow in the core region, turbulent structures emanated from the holes in the perforated plate and occasional bursts of vortex rings in the shear layer. However, incorrect inlet boundary condition can result in unrealistic vortex breakdown phenomenon and subsequent flow reversal in the core region which can dominate the flame stabilization mechanism. Under such circumstances the flow field exhibits the typical characteristics of a high swirl field and the flame is shown to deviate

from low swirl flame characteristics. However, the flame position along the centerline could be well predicted under these circumstances which suggests that one dimensional flame analysis, which is frequently performed in low swirl flame studies, is certainly inadequate and misleading.

Three alternative approaches for specifying the inlet condition were considered. No flame dynamics in the core region were observed when the jets emanated from the holes in the perforated-plate were excluded from computations. Modeling the perforated plate holes as individual non-circular jets at the inlet yielded a dynamic flame in the core region, however correct dynamics were only resolved when the computational domain was extended back to include the perforated plate. This choice of computational domain results in a complicated geometry and large number of grid cells, thus it is not computationally economical. However, it was shown that the velocity fluctuations at the nozzle exit plane are not correlated with the flame front position. Thus a time series of solutions obtained from this simulation can be used as the inlet condition in other LSB simulations. This approach results in a simple cartesian grid which is favorable for all computational codes.

The upwind thickening technique used in this study is based on the same grounds as the artificially thickened flame technique. However, the thickening factor is not decided in advance and numerical stability requirements would automatically choose proper thickening factor, hence unnecessary thickening is avoided. Nevertheless, inadequate thickening increases the error in evaluation of filtered source term in the species mass transport equations which in turn triggers non-linear numerical instabilities.

Studying the unsteady phenomena in PDE revealed that direct substitution of the combustion chamber in a conventional turbofan aircraft engine needs certain re-thinking in turbomachinery design in order to adapt to the intermittent process of pulse detonation. Nonetheless, starless PDE configuration suggested in this work showed a more flexible range of working conditions under such unsteady conditions. The simple finite rate chemistry model successfully predicted the correct detonation speed and flow properties at Chapman-Jouguet plane.

6.1 Future Work

The flame stabilization mechanism suggested in this work is of qualitative nature. Both experimental and numerical data can be further analyzed in order to recognize and quantify flame spatial and temporal structures and to identify certain modes which are possibly more

important in flame stabilization. Analysis of this nature can improve LSB concept toward more robust designs which are capable of working under a variety of operating conditions.

The aim of the laboratory LSB flame studied in the present work is to eventually serve as a test case for numerical studies aimed at evaluation of numerical methods and combustion model. Although the inlet is the most challenging boundary condition, the circumferential boundaries can pose extra difficulties. The co-flow is aimed at keeping this open flame from environmental disturbances, however it is difficult to assure that the co-flow can protect such a delicate dynamic flame from pressure variations present in the laboratory environment. These circumferential boundaries pose difficulties in numerical simulations since the computational domain should be extended to ensure minimum entrainment through these boundaries. Confinement of the flame can address such difficulties both in experimental and numerical studies. Confinement of the LSB flame is eventually inevitable if it is meant to replace current industrial burner technologies.

The swirling jet in the LSB immediately starts to mix in the outer shear layer at the nozzle exit resulting in a region of stratified flow with varying equivalence ratios. The good laminar flame speed predictions of the global mechanism used in this study is limited to the nominal equivalence ratio in the core region while at lower ratios it over predicts the flame speed. This can affect both radial distribution of temperature and flame spatial scales and in extreme cases can modify the flame stabilization mechanism. This discrepancy in laminar flame speed prediction should be treated by either general modification of the global mechanism or by direct modification of the reaction rates during computations based on tabulated data for laminar flame speed versus equivalence ratio. Measured radial profiles of temperature are not yet available and this modification was not carried out in this study due to lack of validations (comparison) data. One other step in combustion model improvement is to elaborate the numerical diffusion approximation as well as using more accurate turbulent flame speed correlations.

It is well known that turbulent flames cause pressure fluctuations. Moreover, numerical instabilities can also generate spurious pressure oscillations. The effects of these pressure variations on the swirling jet stability in LSB are not studied here but can be of importance in flame stabilization. Nevertheless, it is known that these numerical oscillations die out faster in three dimensional simulations and hopefully can not significantly affect the evolution/stability of the swirling jet. However, this is an important phenomenon and needs to be studied separately in a simple geometry.

Although the pulse detonation engine concept has been occasionally considered in the past decades, it is still a young subject from practical point of view. There are numerous topics that can be considered for future work, however adding a rotor row to the computational domain presented in this work seems to be the most natural way to continue the present study. The conventional rotor designs might not be suitable for highly unsteady flow in PDE and an impulse turbine seems to be a better first option.

There are well known loss calculation methods, in form of correlations, for engines under steady state working conditions. PDE on the other hand does not work in such conditions, however time resolved results from CFD can be used to calculate losses in PDE and to predict the overall efficiency of the engine. The equilibrium condition of combustion products is assumed in this study, however dissociation of gases at PDE high temperatures is an important fact. This assumption does not significantly affect the phenomena studied here but it certainly affects PDE efficiency calculations. More complicated reaction mechanisms should be used instead of such simple single reaction mechanism for efficiency analysis.

Bibliography

- AKKERMAN, V. 2007 Turbulent burning, flame acceleration, explosion triggering. PhD thesis, Department of Physics, Umeå University, Umeå, Sweden.
- AMIN, M. R., ROUF, H. Z. & CAMBIER, J.-L. 2005 Numerical investigation on the effects of nozzle geometry on the performance of a pulse detonation engine. *Journal of Mechanical Engineering* **51**, 484–490.
- ANDERSSON, N. 2005 A study of subsonic turbulent jets and their radiated sound using large-eddy simulation. PhD thesis, Department of Applied Mechanics, Chalmers University of Technology, Göteborg, Sweden.
- BÉDAT, B. & CHENG, R. K. 1995 Experimental study of premixed flames in intense isotropic turbulence. *Combustion and Flame* **100**, 485–494.
- BUTLER, T. D. & O’ROURKE, P. J. 1997 A numerical method for two dimensional unsteady reacting flows. *Symposium (international) on combustion* **16**, 1503–1515.
- CALVIN, P. & WILLIAMS, F. 1979 Theory of premixed-flame propagation in large scale turbulence. *Journal of Fluid Mechanics* **90**, 589–604.
- CAMBIER, J.-L. & TENGÉR, J. K. 1998 Strategies for pulsed detonation engine performance optimization. *Journal of Propulsion and Power* **14**, 489–498.
- CHAKRABORTY, P., BALACHANDAR, S. & ADRIAN, R. J. 2005 On the relationship between local vortex identification schemes. *Journal of Fluid Mechanics* **535**, 189–214.
- CHAN, C. K., LAU, K. S., CHIN, W. K. & CHENG, R. K. 1992 Freely propagating open premixed turbulent flames stabilized by swirl. *Proceedings of the Combustion Institute* **24**, 511–518.

- CHARLETTE, F., MENEVEAU, C. & VEYANTE, D. 2002 A power-law flame wrinkling model for les of premixed turbulent combustion. part i: Non-dynamic formulation and initial tests. *Combustion and Flame* **131**, 159–180.
- CHENG, R. K. 1995 Velocity and scalar characteristics of premixed turbulent flames stabilized by weak swirl. *Combustion and Flame* **101**, 1–14.
- CHENG, R. K., LITTLEJOHN, D., NAZEER, W. A. & SMITH, K. O. 2008 Laboratory studies on the flow field and characteristics of low-swirl injectors for adaption to fuel-flexible turbines. *Journal of Engineering for Gas Turbines and Power* **130**, 021501–1–021501–10.
- CHENG, R. K., LITTLEJOHN, D., STRAKEY, P. A. & SIDWELL, T. 2009 Laboratory investigations of a low-swirl injector with h₂ and ch₄ at gas turbine conditions. *Proceedings of the Combustion Institute* **32**, 3001–3009.
- CHENG, R. K., YEGIAN, D. T., MIYASATO, M. M., SAMUELSEN, G. S., BENSON, C. E., PELLIZZARI, R. & LOFTUS, P. 2000 Scaling and development of low-swirl burners for low-emission furnaces and boilers. *Proceedings of the Combustion Institute* **28**, 1305–1313.
- COLIN, O., DUCROS, F., VENYANTE, D. & POINSOT, T. 2000 A thickened flame model for large eddy simulations of turbulent premixed combustion. *Physics of Fluids* **12**, 1843–1863.
- DAY, M., TACHIBANA, S., BELL, J., LIJEWSKI, M., BECKNER, V. & CHENG, R. K. 2012 A combined computational and experimental characterization of lean premixed turbulent low swirl laboratory flames i.methane flames. *Combustion and Flame* **159**, 275–290.
- DOROFEEV, S. B., SIDOROV, V. P., KUZNETSOV, I. D., MATSUKOV, V. I. & ALEKSEEV, V. I. 1999 Effects of scale on the onset of detonation. In *17th International Colloquium on the Dynamics of Explosions and Reactive Systems*. Heidelberg, Germany.
- EBRAHIMI, H. & MERKLE, C. L. 2002 Numerical simulation of pulse detonation engine with hydrogen fuels. *Journal of Propulsion and Power* **18**, 1042–1048.
- ERIKSSON, L.-E. 1995 Development and validation of highly modular flow solver versions in g2dflow and g3dflow series for compressible viscous flow. Internal report 9970-1162. Volvo Aero Corporation, Sweden.

- ERIKSSON, L.-E. 1996 A preconditioned navier-stokes solver for low mach number flows. In *Third ECCOMAS Computational Fluid Dynamics Conference*. Paris, France.
- ERLEBACHER, G., HUSSAINI, M. Y., SPEZIALE, C. G. & ZANG, T. A. 1992 Toward the large-eddy simulation of compressible turbulent flows. *Journal of Fluid Mechanics* **238**, 155–185.
- FICKETT, W. & DAVIS, W. C. 1979 *DETONATION THEORY AND EXPERIMENT*, 1st edn. DOVER PUBLICATIONS.
- GLASSMAN, I. 1996 *Combustion*, 3rd edn. Academic Press.
- GOLDMEER, J., TANGIRALA, V. & DEAN, A. 2008 System-level performance estimation of a pulse detonation based hybrid engine. *Journal of Engineering for Gas Turbines and Power* **130**, 011201–1–011201–8.
- GÜLDER, O. L. 1990 Turbulent premixed flame propagation models for different combustion regimes. *Proceedings of the Combustion Institute* **23**, 743–750.
- HE, X. & KARAGOZIAN, A. R. 2006 Pulse-detonation-engine simulations with alternative geometries and reaction kinetics. *Journal of Propulsion and Power* **22**, 852–861.
- JOHNSON, M. R., LITTLEJOHN, D., NAZEER, W. A., SMITH, K. O. & CHENG, R. K. 2005 A comparison of the flow fields and emissions of high-swirl injectors and low-swirl injectors for lean premixed gas turbines. *Proceedings of the Combustion Institute* **30**, 2867–2874.
- KANG, D. M., CULICK, F. E. C. & RATNER, A. 2007 Combustion dynamics of a low-swirl combustor. *Combustion and Flame* **151**, 412–425.
- KENTFIELD, J. A. C. 2002a Fundamentals of idealized airbreathing pulse-detonation engines. *Journal of Propulsion and Power* **18**, 77–83.
- KENTFIELD, J. A. C. 2002b Thermodynamics of airbreathing pulse-detonation engines. *Journal of Propulsion and Power* **18**, 1170–1175.
- KUO, K. K. 2005 *Principles of Combustion*, 2nd edn. John Wiley Sons.
- LANEY, C. B. 1998 *Computational Gasdynamics*, 1st edn. Cambridge University Press.

Mohammad Irannezhad, *A Numerical Study of Reacting Flows Using Finite Rate Chemistry*

- LEFEBVRE, A. H. 1999 *Gas Turbine Combustion*, 2nd edn. New York: Taylor & Francis.
- LEGIER, J. P., POINSOT, T. & VEYANTE, D. 2000 Dynamically thickened flame les model for premixed and non-premixed turbulent combustion. In *Center for Turbulent research. Proceedings of the summer program 2000*.
- LIPATNIKOV, A. N. & CHOMIAK, J. 2002 Turbulent flame speed and thickness: phenomenology, evaluation and application in multi-dimensional simulations. *Progress in Energy and Combustion Science* **28**, 1–74.
- LITTLEJOHN, D. & CHENG, R. K. 2007 Fuel effects on a low-swirl injector for lean premixed gas turbines. *Proceedings of the Combustion Institute* **31**, 3155–3162.
- LITTLEJOHN, D., MAJESKI, A. J., TONSE, S., CASTALDINI, C. & CHENG, R. K. 2002 Laboratory investigation of an ultralow No_x premixed combustion concept for industrial boilers. *Proceedings of the Combustion Institute* **29**, 1115–1121.
- MA, F., CHOI, J.-Y. & YANG, V. 2005 Thrust chamber dynamics and propulsive performance of single-tube pulse detonation engine. *Journal of Propulsion and Power* **21**, 512–526.
- MAREK, C. J., PAPATHAKOS, L. C. & VERBULECZ, P. W. 1977 Preliminary studies on autoignition and flashback in a premixed prevaporizing flame tube using jet-a fuel at lean premixed equivalence ratios. NASA Technical Memorandum NASA TM X-3526. NASA.
- MCBRIDE, B. J. & GORDON, S. 1996 Computer program for calculation of complex chemical equilibrium compositions and applications ii. user's manual and program description. Nasa rp-1311-p2. NASA.
- MEREDITH, K. V. & BLACK, D. L. 2006 Automated global mechanism generation for use in cfd simulations. In *44th AIAA Aerospace Sciences Meeting and Exhibit*. Reno, Nevada, USA.
- MORRIS, C. I. 2005 Numerical modeling of single-pulse gasdynamics and performance of pulse detonation rocket engines. *Journal of Propulsion and Power* **21**, 527–538.
- NOGENMYR, K.-J. 2008 On the modeling of premixed combustion under varying equivalence ratios. PhD thesis, Division of Fluid Mechanics, Lund University, Lund.

- NOGENMYR, K.-J., FUREBY, C., BAI, X. S., PETERSSON, P., COLLIN, R. & LINNE, M. 2009 Large eddy simulation and laser diagnostic studies on a low swirl stratified premixed flame. *Combustion and Flame* **156**, 25–36.
- NOGENMYR, K.-J., PETERSSON, P., BAI, X. S., FUREBY, C., COLLIN, R., LANTZ, A., LINNE, M. & ALDÉN, M. 2010 Structure and stabilization mechanism of a stratified premixed low swirl burner. *Proceedings of the Combustion Institute* **12**, 1843–1863.
- NOGENMYR, K.-J., PETERSSON, P., BAI, X. S., NAUERT, A., OLOFSSON, J., BRACKMAN, C., SEYFRIED, H., ZETTERBERG, J., LI, Z. S., RICHTER, M., DREIZLER, A., LINNE, M. & ALDÉN, M. 2007 Large eddy simulation and experiments of stratified lean premixed methane/air turbulent flames. *Proceedings of the Combustion Institute* **31**, 1467–1475.
- OLAUSSON, M. 2011 Turbomachinery aeroacoustic calculations using nonlinear methods. PhD thesis, Department of Applied Mechanics, Chalmers University of Technology, Göteborg, Sweden.
- ORAN, E. S. & BORIS, J. P. 2001 *Numerical Simulation of Reactive Flow*, 2nd edn. Cambridge University Press.
- PAXSON, D. E. 2001 A performance map for ideal air breathing pulse detonation engines. NASA Technical Memorandum NASA TM-2001-211085. NASA.
- PETERS, N. 1999 The turbulent burning velocity for large scale and small scale. *Journal of Fluid Mechanics* **384**, 107–132.
- PETERS, N. 2000 *Turbulent Combustion*, 1st edn. Cambridge University Press.
- PETERSSON, P., OLOFSSON, J., BRACKMAN, C., SEYFRIED, H., ZETTERBERG, J., RICHTER, M., ALDÉN, M., LINNE, M. A., CHENG, R. K., NAUERT, A., GEYER, D. & DREIZLER, A. 2007 Simultaneous PIV/OH-PLIF, Rayleigh thermometry/OH-PLIF and stereo PIV measurements in a low-swirl flame. *Applied Optics* **46**, 3928–3936.
- POPE, S. B. 1985 Pdf methods for turbulent reacting flows. *Progress in Energy and Combustion Science* **11**, 119–192.
- POPE, S. B. 1990 Computations of turbulent combustion: Progress and challenges. *Proceedings of the Combustion Institute* **23**, 591–612.

Mohammad Irannezhad, A Numerical Study of Reacting Flows Using Finite Rate Chemistry

- RASHEED, A. & TANGIRALA, V. E. 2004 Interactions of a pulsed detonation engine with a 2d turbine blade cascade. In *42nd Aerospace Sciences Meeting and Exhibit*. Reno, Nevada.
- ROUSER, K. P., KING, P. I., SCHAUER, F. R., SONDERGAARD, R. & HOKE, J. L. 2010 Parametric study of unsteady turbine performance driven by a pulse detonation combustor. In *46th AIAA/ASME/SAE/ASEE Joint Propulsion Conference and Exhibit*. Nashville, TN.
- SAGAUT, P. 2000 *Large Eddy Simulation for Incompressible Flows*, 1st edn. Springer.
- SCHAUER, F. R., MISER, C. L., TUCKER, K. C., BRADLEY, R. P. & HOKE, J. L. 2005 Detonation initiation of hydrocarbon-air mixtures in a pulsed detonation engine. In *43rd AIAA Aerospace Sciences*. Reno, Nevada.
- SCHELKIN, K. L. 1947 NASA Technical Memorandum NO. 1110. NASA.
- SHEPHERD, I. G., CHENG, R. K., PLESSING, T., KORTSCHICK, C. & PETERS, N. 2002 Premixed flame front structure in intense turbulence. *Proceedings of the Combustion Institute* **29**, 1833–1840.
- SIEVERDING, C. H. 1982 Test case 1: 2-d transonic turbine nozzle blade, workshop on 2d and 3d flow calculations on turbine bladings. In *Numerical Methods for Flows in Turbomachinery Bladings*.
- SPADACCINI, L. J. & TEVELDE, J. A. 1980 Autoignition characteristics of aircraft-type fuels. NASA contractor report NASA CR-159886. NASA.
- STRAKEY, P. A. & EGGENSPIELER, G. 2010 Development and validation of a thickened flame modeling approach for large eddy simulation of premixed combustion. *Journal of Engineering for Gas Turbines and Power* **132**, 071501–1–071501–9.
- TANGIRALA, V. E. & RASHEED, A. 2007 Pulsed detonation engine and turbine interactions. In *International Symposium on Air Breathing Engines*. Beijing, China.
- VALIEV, D. M., BYCHKOV, V., AKKERMAN, V. & ERIKSSON, L.-E. 2009 Different stages of flame acceleration from slow burning to chapman-jouguet deflagration. *Physical Review* **80**, 036317–1–036317–11.

- WANG, G., BOILEAU, M. & VEYANTE, D. 2011 Implementation of a dynamic thickened flame model for large eddy simulations of turbulent premixed combustion. *Combustion and Flame* **158**, 2199–2213.
- WINTENBERGER, E. 2004 Application of steady and unsteady detonation waves to propulsion. PhD thesis, California Institute of Technology.
- WU, Y., MA, F. & YANG, V. 2003 System performance and thermodynamics cycle analysis of airbreathing pulse detonation engines. *Journal of Propulsion and Power* **19**, 556–567.
- YAN, J., MOCKETT, C. & THIELE, F. 2005 Investigation of alternative length scale substitutions in detached-eddy simulation. *Flow, Turbulence and Combustion* **74**, 85–102.
- ZANTE, D. V. & TURNER, M. G. 2007 The attenuation of a detonation wave by an aircraft engine axial turbine stage. In *International Symposium on Air Breathing Engines*. Beijing, China.
- ZIMONT, V. L. 2000 Gas premixed combustion at high turbulence. turbulent flame closure combustion model. *Experimental Thermal and Fluid Science* **21**, 179–186.
- ZIMONT, V. L. & LIPATNIKOV, A. 1995 A numerical model of premixed turbulent combustion of gases. *Chemical Physics Reports* **14**, 993–1025.

Appendix A

Preconditioning

THE COMPRESSIBLE flow solver works satisfactorily for moderate to high Mach number flows but when approaching the incompressible limit the efficiency decrease drastically. The CFL number in compressible flow is defined as

$$CFL = \frac{\Delta t}{\Delta x}(|u| + c) \quad (\text{A.1})$$

In the incompressible limit the dominating velocity in the CFL number is the speed of sound c which forces unnecessary small time steps in an explicit solver, hence leading to low efficiency in solving low Mach number flows with a standard compressible flow solver. One way to overcome this problem is to use preconditioning. The idea is to alter the transient behavior of acoustic waves without affecting that of the flow. This is physically meaningful in this type of problems where there is only one way coupling between the flow and acoustics; the acoustic waves have negligible effects on the flow as long as they are *fast enough*. This is achieved by artificially decreasing the speed of acoustic waves. The preconditioning concept used here is based on an isentropic pressure under-relaxation (Eriksson (1996)); to reduce the rate of change of pressure as it is given by regular compressible Navier-stokes equations while applying appropriate corrections to avoid entropy errors. If the under-relaxation factor is chosen correctly the effective speed of acoustic waves will decrease without affecting the convection-diffusion properties. The preconditioning is obtained by modifying the governing equation 3.28 according to

$$M^{-1} \frac{\partial Q}{\partial t} + \frac{\partial \mathcal{F}_j}{\partial x_j} = \mathcal{H} \quad (\text{A.2})$$

Assuming homogeneous inviscid case and writing equation A.2 in primitive variable vector q yields

$$\frac{\partial q}{\partial t} + \tilde{M} \tilde{A}_j \frac{\partial q}{\partial x_j} = 0 \quad (\text{A.3})$$

where

$$q = \begin{bmatrix} \bar{\rho} \\ \tilde{u}_i \\ \tilde{e}_0 \\ \tilde{Y}^{(m)} \\ \tilde{k} \\ \tilde{\varepsilon} \end{bmatrix} \quad (\text{A.4})$$

$$\tilde{A}_j = \frac{\partial q}{\partial Q} \frac{\partial \mathcal{F}_j^{(inv)}}{\partial Q} \frac{\partial Q}{\partial q} \quad (\text{A.5})$$

$$\tilde{M} = \frac{\partial q}{\partial Q} M \frac{\partial Q}{\partial q} \quad (\text{A.6})$$

The idea is to find \tilde{M} so that a pressure under-relaxation level of α is imposed

$$\left(\frac{\partial p}{\partial t}\right)^{new} = \alpha \left(\frac{\partial p}{\partial t}\right)^{calc.} \quad (\text{A.7})$$

where the superscript *calc.* refers to the values calculated from regular Navier-Stokes equations without preconditioning. The rate of change of entropy should be preserved by correcting the rate of change of density according to

$$\left(\frac{\partial \rho}{\partial t}\right)^{new} - \left(\frac{\partial \rho}{\partial t}\right)^{calc.} = \frac{1}{c^2} \left[\left(\frac{\partial p}{\partial t}\right)^{new} - \left(\frac{\partial p}{\partial t}\right)^{calc.} \right] \quad (\text{A.8})$$

The speed of acoustic waves in any arbitrary direction (n_x, n_y, n_z) is reduced to

$$\frac{1}{2}(1 + \alpha)U \pm \sqrt{\frac{1}{4}(1 - \alpha)^2 U^2 + \alpha \delta^2 c^2} \quad (\text{A.9})$$

where

$$U = n_x u + n_y v + n_z w$$

$$\delta = \sqrt{n_x^2 + n_y^2 + n_z^2}$$

and the *CFL* number will decrease consequently, hence allowing larger time steps.

Appendix B

Species Diffusive Flux Approximation

THE DIFFUSIVE flux in species transport equations was approximated using Fick's law and assuming equal Schmidt numbers for all species.

$$J^{(m)} = -\rho D \nabla Y^{(m)} \quad (\text{B.1})$$

Laminar flame calculations for a methane/air mixture at equivalence ratio of $\phi = 0.62$, similar to LSB conditions, were performed using both exact and approximated equations. The Meredith reaction mechanism was used for both cases. The computed flame structure is shown in figure B.1 which indicates that the error in laminar flame structure predictions using this simplified species diffusion flux is small. The computed laminar flame speeds also agree and are $\sim 12.5\text{cm/s}$ and $\sim 13\text{cm/s}$ for approximated and exact methods respectively. The exact solution was calculated using commercial code CHEMKIN and the laminar flame with approximated diffusion term was simulated using the same numerical tool used for all other simulations in this thesis. The grid resolution was 0.01mm , therefore the flame structure is fully resolved (DNS).

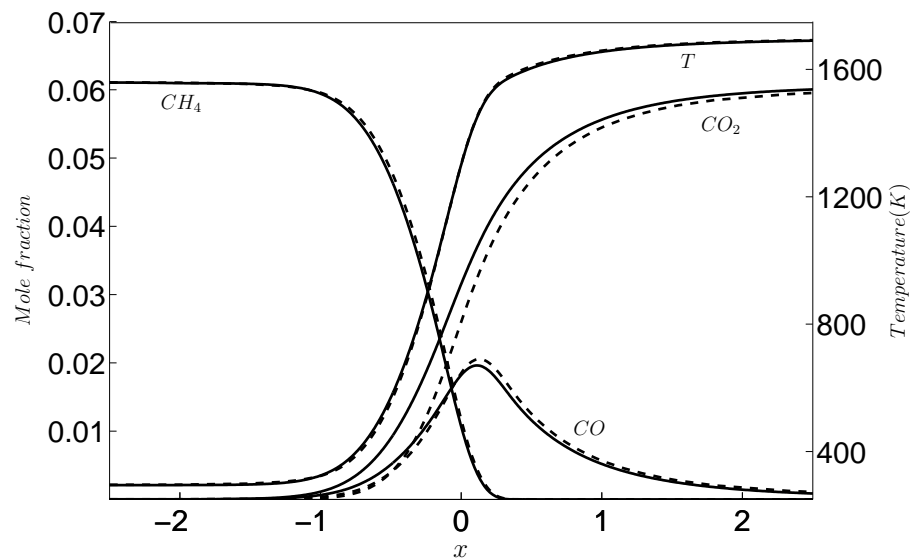


Figure B.1: Structure of lean premixed methane/air flame at $\phi = 0.62$ computed for Meredith global reaction mechanism with exact species diffusion term, dashed lines, and approximated species diffusion term, solid lines.

Appendix C

Hybrid LES/URANS

TREMENDOUS NUMBER of grid cells are needed to resolve the walls in LES simulations. Hybrid LES/RANS models are useful when only the flow unsteady structures far from the walls are of interest. The wall region is then treated with RANS turbulence models and LES is applied elsewhere. It can be shown that $k-\varepsilon$ turbulence model works as a Smagorinsky subgrid scale LES model if a proper upper limit on the turbulent length scale is imposed. Under such conditions, the model works as Smagorinsky model everywhere except close to solid walls. Here it is shown how $k-\varepsilon$ turbulence model behaves as Smagorinsky subgrid model under such circumstances (Olausson (2011)). Yan *et al.* (2005) did similar work for a $k-\omega$ model.

The turbulent viscosity is defined as

$$\mu_t = C_\mu \bar{\rho} \frac{\tilde{k}^2}{\tilde{\varepsilon}} \quad (\text{C.1})$$

without the realizability constraint. The turbulent length scale is defined as

$$l_t = C_\mu^{3/4} \frac{\tilde{k}^{3/2}}{\tilde{\varepsilon}} \quad (\text{C.2})$$

Taking only the turbulence part of the viscous stress tensor from equation (3.31) gives:

$$\tau_{ij}^{(t)} = \mu_t \left(2\tilde{S}_{ij} - \frac{2}{3} \frac{\partial \tilde{u}_k}{\partial x_k} \delta_{ij} \right) - \frac{2}{3} \bar{\rho} \tilde{k} \delta_{ij} \quad (\text{C.3})$$

Since the stress tensor is symmetric, the turbulence production term can be written as

$$P_k = \tau_{ij}^{(t)} \frac{\partial \tilde{u}_i}{\partial x_j} = \left\{ \begin{array}{l} \tau_{ij}^{(t)} = \\ \text{Symmetric} \end{array} \right\} = \tau_{ij}^{(t)} \tilde{S}_{ij} \quad (\text{C.4})$$

If compressibility effects are moderate, we may approximate the stress tensor as

$$\tau_{ij}^{(t)} = 2\mu_t \tilde{S}_{ij} \quad (\text{C.5})$$

which gives:

$$P_k = 2\mu_t \tilde{S}_{ij} \tilde{S}_{ij} \quad (\text{C.6})$$

It is safe to assume equilibrium conditions for subgrid scale turbulence, which means that the turbulence production equals dissipation:

$$P_k = \bar{\rho} \tilde{\varepsilon} \quad (\text{C.7})$$

The dissipation can then be written as

$$\tilde{\varepsilon} = \frac{2\mu_t}{\bar{\rho}} \tilde{S}_{ij} \tilde{S}_{ij} \quad (\text{C.8})$$

Far from the walls the turbulent length scale given by equation C.2 is large and exceeds the upper limit $l_{t,max}$, therefore turbulent dissipation $\tilde{\varepsilon}$ would be given by algebraic equation C.9.

$$\tilde{\varepsilon} = C_\mu^{3/4} \frac{\tilde{k}^{3/2}}{l_{t,max}} \quad (\text{C.9})$$

Combining equation (C.8) with equation (C.9) gives:

$$C_\mu^{3/4} \frac{\tilde{k}^{3/2}}{l_{t,max}} = \frac{2\mu_t}{\bar{\rho}} \tilde{S}_{ij} \tilde{S}_{ij} \quad (\text{C.10})$$

Using equation (C.9) μ_t can be expressed as follows:

$$\mu_t = C_\mu \bar{\rho} \frac{\tilde{k}^2}{\tilde{\varepsilon}} = l_{t,max} C_\mu^{1/4} \bar{\rho} \sqrt{\tilde{k}} \quad (\text{C.11})$$

Equations (C.10) and (C.11) give:

$$C_\mu^{3/4} \frac{\tilde{k}^{3/2}}{l_{t,max}} = \frac{2 l_{t,max} C_\mu^{1/4} \bar{\rho} \sqrt{\tilde{k}}}{\bar{\rho}} \tilde{S}_{ij} \tilde{S}_{ij} \quad (\text{C.12})$$

Rearranging this equation gives an expression for the turbulence kinetic energy:

$$\tilde{k} = \frac{2}{\sqrt{C_\mu}} l_{t,max}^2 \tilde{S}_{ij} \tilde{S}_{ij} \quad (\text{C.13})$$

Combining equation (C.11) with equation (C.13) gives an expression for the turbulence viscosity:

$$\mu_t = \sqrt{2} \bar{\rho} l_{t,max}^2 \sqrt{\tilde{S}_{ij} \tilde{S}_{ij}} \quad (\text{C.14})$$

Replacing μ_t in equation (C.8) with the expression in equation (C.14) gives:

$$\tilde{\varepsilon} = 2\sqrt{2}l_{t,max}^2 \left(\tilde{S}_{ij}\tilde{S}_{ij} \right)^{3/2} \quad (C.15)$$

In Smagorinsky model (incompressible version) the turbulent viscosity is given by

$$\mu_t = \rho (C_S \Delta f)^2 \sqrt{2 \tilde{S}_{ij}\tilde{S}_{ij}} \quad (C.16)$$

where C_S is a constant between 0.065 and 0.25 depending on the flow and Δf is the filter width.

Comparing the expressions for μ_t , equation (C.14) and (C.16), reveals that far from the walls where the upper limit on turbulent length scale is activated the turbulent viscosity given by $k - \varepsilon$ model is equal to Smagorinsky model if

$$l_{t,max} = C_S \Delta f \quad (C.17)$$

Therefore, by choosing a proper value for $l_{t,max}$ the $k - \varepsilon$ turbulence model behaves as Smagorinsky subgrid LES model far from the walls.

